DIFFERENTIAL RECTIFICATION OF SLR-IMAGES USING MAP-DERIVED AND RADAR-GENERATED DIGITAL ELEVATION MODELS

G. Domik, F. Leberl, J. Raggam

Technical University
and Graz Research Center
A-8010 Graz, Austria

29 February 1984

DIBAG Report Nr. 17

1.0 INTRODUCTION 1
2.0 REVIEW OF SINGLE IMAGE RADARGRAMMETRY FOR RECTIFICATION 3
2.1 Image Coordinates 3
2.2 Projection Equation 5
2.3 Inner Orientation 9
2.4 Relating Image And Object 10
2.4.1 Interpolative Methods 11
2.4.2 Parametric Models 15
2.4.3 Hybrid Methods 19
2.5 Projection Of A Ground Control Point Into A Radar Image 19
2.6 Rectification 22
2.7 Past Accuracy Studies 23
3.0 DESCRIPTION OF A SYSTEM FOR DIGITAL RADAR IMAGE RECTIFICATION 28
3.1 General 28
3.2 Radar Rectification Based On Simulation 29
4.0 GENERATING A DEM WITH RADAR STEREO MAPPING 32
4.1 Background 32
4.2 Overview Of System Modules 33
4.3 Radar Stereo Model Set-up 34
4.4 Example Of Radar Stereo Plotting With SIR-A Satellite Data 37
4.5 Software Implementation 41
5.0 RADAR IMAGE SIMULATION 42
5.1 The Geometric Imaging Model 42
5.2 Radiometric Model Of Imaging 45
5.3 Data Structure 46
5.4 Software Implementation 47
6.0 OTHER AUXILIARY SYSTEM ELEMENTS 49
6.1 Registration 49
6.2 Removing Geometric Radar Distortions 50
7.0 EXAMPLES OF RADAR IMAGE RECTIFICATION 52
7.1 Oetztal-Data 52
7.2 Processing Of The Oetztal Data 54
7.3 Cephalonia Data 59
7.4 Processing Of Cephalonia Data 59
8.0 CONCLUSION AND OUTLOOK 63

Acknowledgement

Work for this report has been made possible through the support and sponsorship of the U.S. Government through its European Research Office, under contract No. DAJA 45-83-C-0018.

ABSTRACT

A multi-step approach to rectify radar images geometrically and radiometrically is presented. The method uses digital elevation models (DEMs) and an image simulator to establish the relation between radar image coordinates and ortho image locations. The simulation serves to create a synthetic gray value image similiar in its geometry to the real radar image, associating with each image pixel a backscatter value dependent on the incidence angle and a DEM address. Correlation between simulated and real image results in a relation between radar backscatter values and DEM addresses and produces an ortho-image in an additional step.

Stereo-derived and map-derived elevation models were used to demonstrate the rectification process for air- and spaceborne radar images.

1.0 INTRODUCTION

Numerous remote-sensing applications are based on precisely relating the gray values of an aircraft or satellite image to the corresponding phenomenon on the ground, to gray values of other images, or to symbolic descriptions of an object in the form of maps.

One concept to solve this correspondence problem is by physically generating a derived image that is geometrically corrected and therefore has the geometric properties of a map. The result can be denoted by "ortho-images" or by "geo-coded imagery". The first expression results from standard photogrammetric terminology where since about 1955 the ortho-photo has become a routine product (Manual of Photogrammetry, 1944). "Geo-coding" is a more recent terminology that was independently developed in the remote-sensing and image processing fields (Guertin, Shaw, 1981).

The generation of digital geo-coded ortho-images requires that given raw input images are resampled in a digital image processing system. Resampling must result in a new output image so that the image gray value of each imaged object is presented in its proper position. Essentially therefore one has to shift input image positions x, y into output positions X, Y such that

- effects of the sensor position and attitude during image acquisition;
- effects of perturbations of the internal sensor operations;
- effects of the imaging characteristics or type of geometric projection;
- effects of the object shape

are all eliminated from the image geometry. The resulting output image has a specified geometry that is independent of the specifics of sensor and image acquisition.

This report describes one procedure to take a digital radar image, recordings of the position and attitude of the sensor platform, and a description of terrain shape in the form of a digital elevation model (DEM), to obtain a digital

ortho-radar image. The approach is based on a pixelwise re-arrangement of the input data; therefore one can refer to the procedure as "differential rectification".

As a by-product of geometric rectification one can also manipulate the image gray values themselves in a step of "radiometric rectification", thereby eliminating image gray value effects of topographic terrain slopes.

The report will first review the current understanding of radar rectification and single image radargrammetry. It will then discuss the individual steps of the rectification procedure developed in the current context, and finally demonstrate results using aircraft and satellite images, both with map-derived and with stereo-radar terrain elevation data.

2.0 REVIEW OF SINGLE IMAGE RADARGRAMMETRY FOR RECTIFICATION

2.1 Image Coordinates

Radargrammetry requires first of all that the radar measurements, time t and slant range r, are properly extracted from the radar recording. This implies some transformation of an image coordinate pair, x, y or pixel line and sample numbers, i,j, into r and t. The basic concept is illustrated in Figure 2.1.

We measure for each image point P its x_k, y_k comparator coordinates or, if we deal with a digital image, its corresponding line and sample numbers. These need to be converted to the time, t, when object P was imaged (sensor events time), and range, r, to P. Numerous methods exist to relate x_k, y_k to r,t. Generally we may therefore just define an operator F:

$$r = F_r(x_k, y_k)$$
$$t = F_t(x_k, y_k) \qquad (2.1)$$

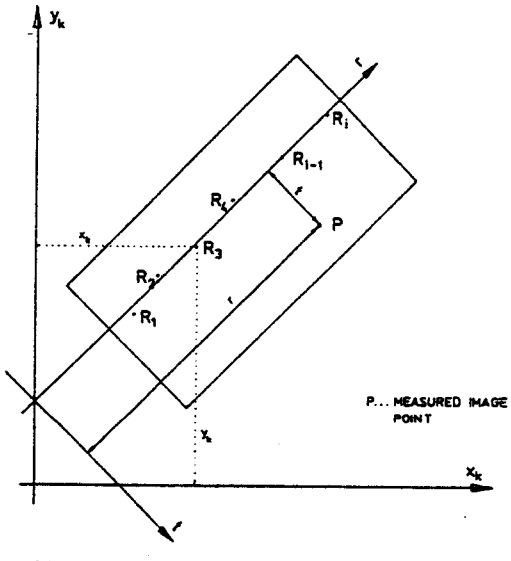

FIGURE 2.1: Measuring coordinates in a side-looking radar image; x_k, y_k are comparator coordinates, r,t are range and time coordinates.

In certain types of radar images, particularly those designed for good geometry, one may find auxiliary reference marks, such as those of Figure 2.1, denoted by R_1, R_2 etc. Depending on the type of marks we can define the form of Equ. (2.1) and its parameters. As an example, a single row of so-called time-marks may enable one to define a straight line to be denoted as "image time coordinate" axis, x.

Numerous methods could be defined to actually implement operators F_r, F_t. Factors to be considered are the type of geometric referencing, the type of radar record in a slant or ground range presentation, the individual digital or electronic pre-processing of the image data etc.

In most cases, radargrammetry begins with the SLR-image, not with the raw electronic signals acquired by the antenna.

However, a trend in digital radar systems is developing to be beyond the radar record and to look into raw, unprocessed signals. First indications are visible in studies by Kratky (1979), Brown et al. (1981) and Curlander et al. (1981). These new approaches rely on concepts such as "sensor events time", i.e. the exact time when a raw pulse was transmitted from and received by the radar antenna, and how the raw radar echo is converted into image points.

Data from the SEASAT-SAR experiment can serve to illustrate the problem of extracting t, r from the image.

For a long time the digitally correlated SEASAT-SAR images did not show any time or range reference marks. The user was not provided with means to enable him to relate, x, y to t, r coordinates. However, Curlander (1981) recently established a relationship that exists between, on one hand, the sensor events time t and slant range r and on the other hand, the image pixel line (azimuth) number i and sample (range) number j. This relationship is for digitally correlated SEASAT-SAR rather complex. This is illustrated by the formulas that were presented by Curlander (1981), who went back to the raw signal data to define r, t for each pixel.

2.2 Projection Equation

Numerous authors have formulated rigorous radar projection equations, similar to the so-called rigorous photogrammetric equations for photography. The intent of these formulations is to model the typical range projection. Object points are projected along concentric circles onto a projection plane (Figure 2.2). Authors who have contributed here are Rinner (1948), Konecny and Derenyi (1966), Rosenfield (1968), Akowetzki (1968), Derenyi (1970), Gracie et al. (1970), Leberl (1970), Hockeborn (1971), Norvelle (1971), Geier (1972), Greve and Cooney (1974), DBA-Systems (1974) and many authors since. A review was compiled by Leberl (1976b).

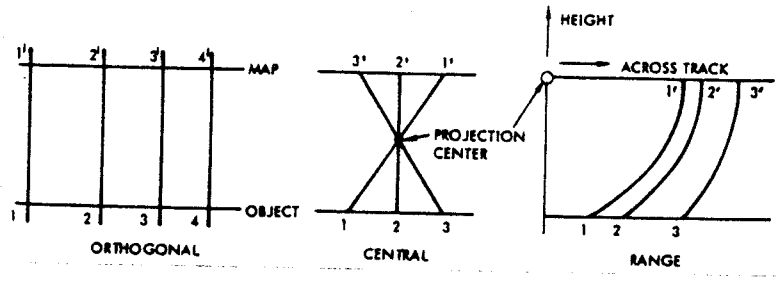

FIGURE 2.2: Range projection. Each image point defines a circle as the locus of the corresponding object point.

For such a formulation we need to define the sensor position, $\underline{s}(t) = (s_x(t), s_y(t), s_z(t))^T$, and antenna attitude with $\phi(t)$, $\omega(t)$, $\kappa(t)$. In synthetic aperture radar, the synthetic antenna's attitude is merely the first derivative of position, namely the velocity vector $\dot{\underline{s}}(t) = (\dot{s}_x(t), \dot{s}_y(t), \dot{s}_z(t))$. Both $\underline{s}(t)$ and $\dot{\underline{s}}(t)$ are functions of time t. The formulation also requires a definition of object- and sensor coordinate systems according to Figure 2.3 with unit vectors $\underline{e}_1$, $\underline{e}_2$, $\underline{e}_3$ and $\underline{u}$, $\underline{v}$, $\underline{k}$, respectively.

We then find for an object point P its position vector $\underline{p}$:

$$\underline{p} = p_x\underline{e}_1 + p_y\underline{e}_2 + p_z\underline{e}_3 \qquad (2.2)$$

and in the sensor system

$$\underline{r} = u_p\underline{u} + v_p\underline{v} + w_p\underline{w} \qquad (2.3)$$

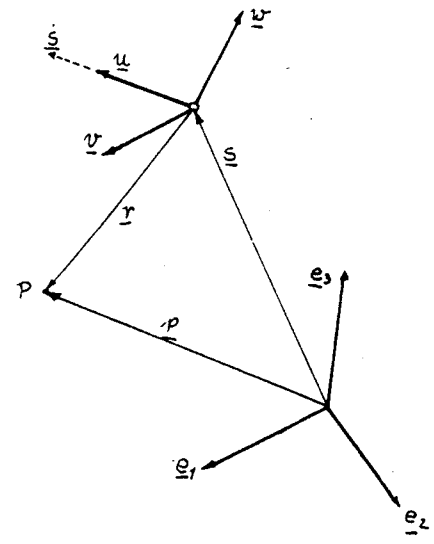

FIGURE 2.3: Definition of object space and sensor coordinate systems.

Therefore,

$$\underline{p} = \underline{s} + \underline{r} \tag{2.4}$$

It is straight forward to see from Figure 2.4 that

$$\begin{aligned} u_p &= r \sin\tau \\ v_p &= r(\sin^2\Omega - \sin^2\tau)^{1/2} \\ w_p &= - r \cos\Omega \end{aligned} \tag{2.5}$$

Auxiliary angle τ is a system constant called squint-angle by most authors (Rosenfield, 1968; Hockeborn, 1971) and defines the conical shape of the radar pulse.

Introducing a new vector $\bar{\underline{p}} = (u_p, v_p, w_p)$ in the sensor coordinate system and a rotation matrix $\underline{A}$ to rotate the sensor system $\underline{u}$, $\underline{v}$, $\underline{w}$ into the object system $\underline{e}_1$, $\underline{e}_2$,

$\underline{e}_3$, we find in matrix notation:

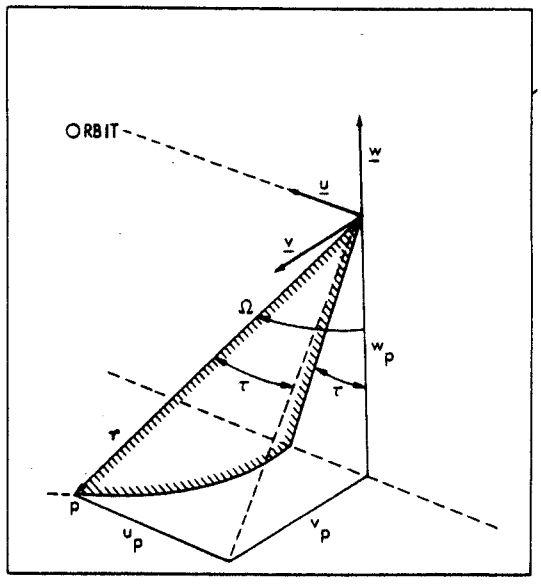

FIGURE 2.4: Relating squint angle τ, slant range r and elevation angle Ω to sensor coordinates u, v, w.

$$\underline{p} = \underline{s} + \underline{A} \cdot \bar{\underline{p}} \tag{2.6}$$

where

$$\underline{A} = \begin{bmatrix} u_x(t) & u_y(t) & u_z(t) \\ v_x(t) & v_y(t) & v_z(t) \\ w_x(t) & w_y(t) & w_z(t) \end{bmatrix} \tag{2.7}$$

Rotation matrix $\underline{A}$ can contain the classical orientation angles ϕ , ω and κ if we deal with a real antenna. With synthetic antennas, we obtain:

$$\underline{u} = (u_x, u_y, u_z) = \dot{\underline{s}}/|\dot{\underline{s}}|$$
$$\underline{v} = (v_x, v_y, v_z) = (\underline{s} \times \dot{\underline{s}})/|\underline{s} \times \dot{\underline{s}}| \qquad (2.8)$$
$$\underline{w} = (w_x, w_y, w_z) = (\underline{u} \times \underline{v})/|\underline{u} \times \underline{v}|$$

The unit vector $\underline{u}$ extends along the synthetic antenna, thus in the direction of the velocity vector $\dot{\underline{s}}$. The unit vector $\underline{v}$ should be normal to $\underline{u}$ and to the nadir direction of the antenna. For satellite sensor, the nadir direction is easily seen to be the direction of the sensor position vector in a planetocentric system. With aircraft radar, one has to specify here explicitly that a geocentric system is assumed also for the sensor position vector $\underline{s}$ and the object coordinate system defined by $\underline{e}_1$, $\underline{e}_2$, $\underline{e}_3$.

Equations (2.5) and (2.6) relate object and image, where r and time t derive from the image coordinates. We now see that - contrary to classical photogrammetry - we do not algebraically relate image and object coordinates, but the image only defines time, which in turn defines the parameters $\underline{s}$ and $\underline{A}$ of Eq. (2.6).

If the imaging arrangement, and thus $\underline{s}(t)$, $\underline{A}(t)$, are known (measurement of navigation data), then we have for each point 3 equations (Eq. 2.5) with 4 unknowns i.e. Ω, p_x, p_y and p_z. It may be preferable to work with 2 equations and 3 unknowns. This is achieved by elimination of the unknown elevation angle Ω (angle between nadir and line of sight), thus giving the following two equations:

$$|\underline{p} - \underline{s}| = r \qquad (2.9)$$

$$\underline{u} \cdot (\underline{p} - \underline{s}) = \sin\tau\, |\underline{u}|\, |\underline{p} - \underline{s}| = \sin\tau \cdot r \qquad (2.10)$$

where we now have a simple geometric description of the radar projection case. The geometric locus of a point is the intersection of range-sphere (Eq. 2.9) with a cone (Eq. 2.10). This is the circular projection line mentioned before.

In Eq. (2.10) the sensor coordinate axes are all described by the geometric position and velocity vector of the antenna. This applies in particular for SAR, since the

antenna attitude is defined by the velocity vector, (the "synthetic" antenna extends in the direction of the physical antenna's motion). For real aperture radar, the real antenna's attitude itself is to be used to define $\underline{u}$, $\underline{v}$ and $\underline{w}$. Therefore angles ϕ and κ must be entered in Eq. (2.7); ω is insignificant and can be set at zero. This is obvious from Eqs. (2.9) and (2.10) which do not contain an angle ω since the components of vector $\underline{u}$ in the rotation matrix $\underline{A}$, namely u_x, u_y and u_z do not contain ω. The same fact is also obvious from geometry: the projection circle is not affected by a sensor roll, ω.

In aircraft radar, τ normally is zero, so the cone of Eq. (2.10) degenerates to a scanning plane:

$$\underline{u} \cdot (\underline{p} - \underline{s}) = 0 \qquad (2.11)$$

The range sphere has an obvious physical explanation: the echo-time measurement of radar clearly associates with each image point a slant range r, and therefore a sphere, as one geometric locus for the corresponding object.

2.3 Inner Orientation

The parameters of the relationship between image coordinates x, y and the object space entities r, t are denoted as parameters of interior orientation. Equation (2.1) was a mathematical representation of this interior orientation. The concept derives from photogrammetric cameras, where each image point defines a projection ray attached to the camera. The exterior orientation relates the projection ray to the object point.

However, Eq. (2.1) represents merely a model of reality. Errors of this model must be anticipated as shown in Figure 2.5. Of course, any error model has unknown coefficients and the question is how to obtain estimates of these coefficients. As will be shown later, these can derive from known object point coordinates. Error models generally imply a polynomial form of the image coordinate deformation Δr, Δt. Gracie et al. (1970), Leberl (1971), DBA-Systems (1974) and others have applied the following polynomials:

$$\Delta r = a_1 r + a_2 r^2 + a_3 r^3 + \ldots$$

$$\Delta t = b_o + b_1 \cdot t + b_2 \cdot t^2 + b_3 \cdot t^3 \qquad (2.12)$$

Little research exists on the various alternatives available to describe Δr, Δt-errors in an optimum form. At this point one can therefore only direct attention to the fact that these errors must be somehow considered in radargrammetry and image rectification.

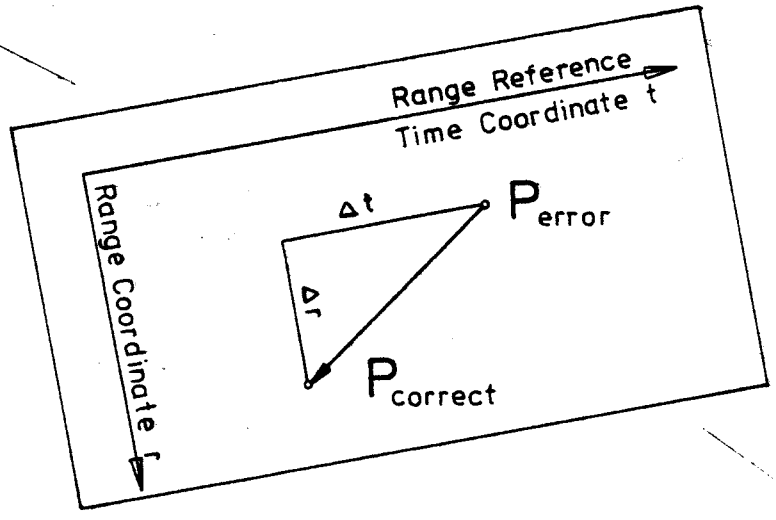

FIGURE 2.5: Radar interior orientation and image deformations Δr, Δt.

2.4 Relating Image And Object

With a given radar image and collateral imaging data we have several options to relate the image to the map or object. We generally will have one unknown or at least only erroneous exterior orientation. This leads to the necessity of using control points or - more generally - control

information to relate image and object space. This has been attempted by many authors. The efforts can be classified into:

a) interpolative models employing so-called "rubber-sheeting" or warping algorithms to make the image fit to ground control;

b) parametric models employing projection equations and computing unknown parameters from control point information; and

c) hybrid combination of a) and b), where the projection equations are used to relate image and object, but where an interpolative technique is applied to represent unknown deviations of reality from the assumed model.

2.4.1 Interpolative Methods

A first approach to the study of image geometry is to consider the image itself as a map substitute and to analyse its differences from a map of known geometric properties. Differences Δx_i, Δy_i between image x_i, y_i and map X_i, Y_i coordinates can be measured at control points i. Some interpolation function is then used to predict Δx_p, Δy_p deformations of the image at arbitrary image locations p. The same methods can be employed as those used in other photogrammetric interpolation tasks (Leberl, 1975). To give but two examples, let us consider Figure 2.6. The points P_i, $i=1,\ldots,n$ are known with their image coordinates x_i, y_i, and map coordinates X_i, Y_i.

(a) Polynomials

We may now, as one example, attempt a scale fit:

$$\begin{bmatrix} X_i \\ Y_i \end{bmatrix} = \begin{bmatrix} a_{11} & a_{12} \\ -a_{12} & a_{11} \end{bmatrix} \begin{bmatrix} x_i \\ y_i \end{bmatrix} \qquad (2.13)$$

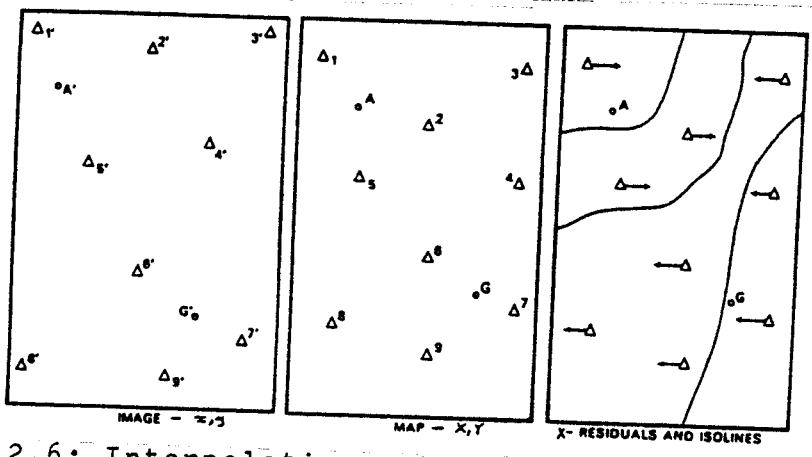

FIGURE 2.6: Interpolative method of relating image and map points; a preliminary transformation leads to residuals ΔX, ΔY. These define a correction surface that can be described by isolines, separately for ΔX and for ΔY.

Since this is solved with more control points than needed one obtains residuals ΔX, ΔY or, if Eq. (2.13) is applied inversely, Δx, Δy. For a new point, x_p, y_p we find thus first X'_p, Y'_p and we obtain the final map coordinates by adding ΔX_p, ΔY_p:

$$\begin{aligned} X_p &= X'_p + \Delta X_p \\ Y_p &= Y'_p + \Delta Y_p \end{aligned} \qquad (2.14)$$

where ΔX_p, ΔY_p result from:

$$\begin{aligned} \Delta X_p &= a_o + a_1 X_p + a_2 Y_p + a_3 X_p Y_p + a_4 Y_p^2 + \ldots \\ \Delta Y_p &= b_o + b_1 X_p + b_2 Y_p + b_3 X_p Y_p + b_4 X_p^2 + \ldots \end{aligned} \qquad (2.15)$$

The coefficients $a_0,\ldots,a_n$, $b_0,\ldots,b_n$ are computed from the known control point values ΔX_i, ΔY_i.

Various authors have evaluated different types of polynomials for radar image correction (Leberl, 1970; Derenyi, 1974a; Hirsch and van Kuilenburg, 1976; Shakine and LeToan, 1978). A common conclusion is difficult to draw, since different data from different sensors were employed. However, one may summarize that the use of polynomials is generally not advisable due to their predictably unfavourable behavior in the case of irregular control point distribution, and in the case of extrapolation. Polynomials are only recommended if they are of low order (1st or second) and if there is an even control point distribution.

(b) Moving average

The polynomials of Eq. (2.15) are a global, closed representation of image deformation. There are also point-wise methods of describing this deformation. We start from the known set of ΔX_i, ΔY_i-values in control points, and need to compute the ΔX_p, ΔY_p in a new point X_p, Y_p. The moving average technique assembles for each point P a set of known control points according to some criterion. This may for example be the n closest control points (Figure 2.7), or it may be m control points in each of four quadrants (Figure 2.8).

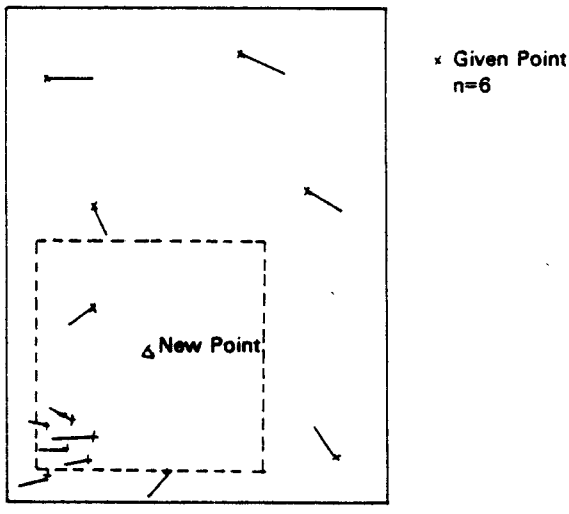

FIGURE 2.7: Moving average interpolation with square windows to collect n reference points.

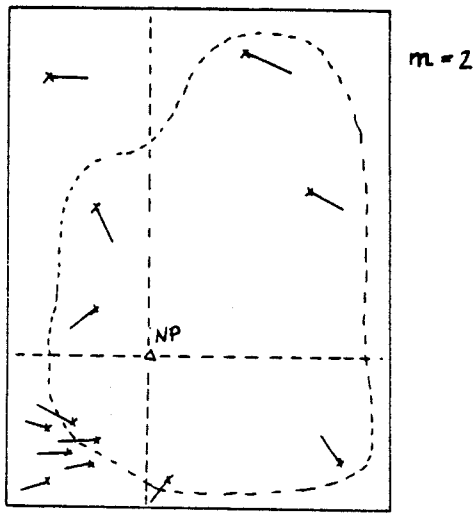

FIGURE 2.8: Selection of control points in quadrants, in this example with 2 points per quadrant.

With these selected control point sets a polynomial of low order is now computed (1st and 2nd order) whereby each control point obtains a weight as a function of its distance from the new point. If all coordinates have been reduced to an origin in the new point, then only the first coefficients a_0, b_0 of this polynomial need to be computed:

$$\Delta X_p = a_o + a_1 X'_p + \ldots$$

$$\Delta Y_p = b_o + b_1 Y'_p + \ldots$$

since X'_p, $Y'_p = 0$.

This computation and control point selection is repeated for each new point. In the case of a first order polynomial one also has the expression "moving plane" interpolation. A zero-order polynomial leads to a simple weighted average interpolation.

2.4.2 Parametric Models

The exterior orientation of the sensor is a function of time and therefore continuously changing. As a result each image-x-coordinate relates to a different exterior orientation. It is obvious that there cannot be rigorous reconstruction of the exterior orientation from control points for all times t: the number of unknown exterior orientation elements is infinite. Even if we had several control points imaged at one given time t and thus along one line in the image-y-direction, complete computation of the exterior orientation is not possible.

To illustrate the problem let us assume that the exterior orientation is nearly perfect and that the flight only slightly deviates from a straight line along the object $\underline{e}_1$-coordinate axis. Also ϕ , ω , κ , the elements of the sensor attitude, are nearly zero.

These small deviations $d\phi$, $d\omega$, $d\kappa$, ds_x, ds_y and ds_z of the sensor from a predictable exterior orientation can be related to image coordinate errors, dr, dt, or dx, dy. We start from Eqs. (2.5) and (2.6):

$$\bar{\underline{p}} = \underline{A}^{-1} \cdot (\underline{p} - \underline{s}) \qquad (2.16)$$

Differentiation of Eq. (2.16) leads to:

$$d\underline{\bar{p}} = d\underline{A}^{-1}(\underline{p} - \underline{s}) - \underline{A}^{-1} \cdot d\underline{s} \qquad (2.17)$$

where $d\underline{s} = (ds_x, ds_y, ds_z)$. Since we assume $\phi=\omega=\kappa \approx 0$, we get $\underline{A}^{-1}$ to be the unit matrix, $\underline{E}$.

The differential form $d\underline{A}^{-1} \cdot (\underline{p} - \underline{s})$ is well known in photogrammetry (Rinner and Burkhardt, 1972):

$$d\underline{A}^{-1} \cdot (\underline{p}-\underline{s}) = \begin{bmatrix} 0 & -d\kappa & d\phi \\ d\kappa & 0 & -d\omega \\ -d\phi & d\omega & 0 \end{bmatrix} \underline{A}^{-1}(\underline{p}-\underline{s}) \qquad (2.18)$$

Therefore we get with $\underline{A}^{-1} \cdot (\underline{p} - \underline{s}) = (u_p, v_p, w_p)^r$:

$$\begin{bmatrix} du_p \\ dv_p \\ dw_p \end{bmatrix} = \begin{bmatrix} -d\kappa \cdot v_p + d\phi \cdot w_p - ds_x \\ d\kappa \cdot u_p - d\omega \cdot w_p - ds_y \\ -d\phi \cdot u_p + d\omega \cdot v_p - ds_z \end{bmatrix} \qquad (2.19)$$

Errors of image x,y-coordinates result from du_p, dv_p and dw_p as follows:

$$dx = du_p$$

But $y=r=(v_p{}^2+w_p{}^2)^{1/2}$. Therefore:

$$dy = dr = \frac{1}{r}(v_p \cdot dv_p + w_p \cdot dw_p)$$
$$= \sin\Omega \cdot dv_p - \cos\Omega \cdot dw_p$$

Let us now simplify further with squint angle $\tau=0$. Then $u_p=0$, $v_p=r \cdot \sin\Omega$ and $w_p=-r \cdot \cos\Omega$. Thus

$$dy = \sin\Omega(-d\omega \cdot w_p - ds_y) - \cos\Omega(d\omega \cdot v_p - ds_z)$$

$$dy = + d\omega \sin\Omega \cdot r \cdot \cos\Omega - \sin\Omega \, ds_y$$

$$- \cos\Omega \, d\omega \cdot r \cdot \sin\Omega + \cos\Omega \, ds_z \qquad (2.20)$$

$$dy = - \sin\Omega \, ds_y + \cos\Omega \, ds_z$$

$$dx = - r \cdot \sin\Omega \, d\kappa - r \cdot \cos\Omega \, d\phi - ds_x$$

With flying height $H = r \cdot \cos\Omega$, or with object coordinates $p_y = r \cdot \sin\Omega$, this can be rewritten:

$$dx = - ds_x + p_y \cdot d\kappa - H \cdot d\phi$$

$$dy = - p_y / r \, ds_y + H / r \cdot ds_z \qquad (2.21)$$

We see again that we have only five elements of exterior orientation. The sixth element, d , has no effect on image geometry.

For each image-x-coordinate, a complete set of five orientation elements must be solved. This is not possible with a co-linear arrangement of control points, since clearly the effects of ds_x and $d\phi$ cannot be separated. We can solve either (ds_x, ds_y, ds_z, $d\kappa$) or ($d\phi$, ds_y, ds_z, $d\kappa$). The fifth element must be known. The required number of control points to compute the four elements is two.

It is unrealistic, however, to assume that for each image x-line one can have two control points. Also this is not necessary because of correlation that exists between the exterior orientation values at two different times t_1 and t_2.

Authors have in the past proposed various mathematical models for the exterior orientation as a function of time, e.g. DBA-Systems (1974) employed polynomials such that:

$$d\phi(t) = a_o + a_1 t + a_2 t^2 + \ldots$$

$$ds_z(t) = f_o + f_1 t + f_2 t^2 + \ldots \qquad (2.22)$$

Instead of solving $d\phi$, $d\kappa$, ds_x, ds_y and ds_z one solves for unknown polynomials coefficients a_0, $a_1, \ldots$ $_0$, $_1, \ldots$ Eq. (2.21) is thus rewritten:

$$
\begin{aligned}
dx = & - \{c_o + c_1 t + c_2 t^2 + \ldots\} \\
& + p_y \cdot \{b_o + b_1 t + b_2 t^2 + \ldots\} \\
& - H \cdot \{a_o + a_1 t + a_2 t^2 + \ldots\} \qquad (2.23) \\
dy = & - \frac{p_y}{r} \cdot \{d_o + d_1 t + d_2 t^2 + \ldots\} \\
& + \frac{H}{r} \cdot \{e_o + e_1 t + e_2 t^2 + \ldots\}
\end{aligned}
$$

Not all coefficients can be determined separately. The analysis of this approach is beyond the scope of this paper. It may, however, be relevant to point out that instead of single high order polynomials it is preferable to use piecewise polynomials of low order. Baker and Mikhail (1974) have studied these approaches, however, for aircraft scanner imagery, not for radar.

Dowideit (1977) studied the method of modelling the exterior orientation parameters by Fourier series, correctly arguing that the elements of the exterior orientation have a periodical behavior with several dominating frequencies (Leberl, 1972a). Again, one has to solve for unknown coefficients of the Fourier series. The main problem is instability of the resulting equation system due to correlation among coefficients.

A somewhat different approach has been proposed for dynamic scanner images by Ebner and Hoessler (1978). The elements of exterior orientation are considered to form time-series appropriately modelled by Gauss-Markoff-chains of order m:

$$\phi(t_{n+1}) = \sum_{i+1}^{m} a_i \phi(t_{n-m+i}) + \varepsilon_{n+1} \qquad (2.24)$$

Thus the exterior orientation is described at discrete times $t_1, t_2, \ldots$; at time t_n, the orientation parameter is

considered to be a linear extrapolation from m previous times plus a random addition, ε. Ebner and Hoessler could show that a numerically stable and comparatively manageable solution can be formulated. A detailed description is beyond the scope of this paper. An application to radar must still be investigated.

2.4.3 Hybrid Methods

A combination of parametric and interpolative methods is feasible and common in photogrammetry. A mathematically rigorous model of the imaging process, such as used in the parametric case, may not be able to describe the entire chain of physical events leading to the image. Unknown elements or effects must be considered. This can be done by introducing Δx, Δy-corrections to the image coordinates; these corrections can be represented by polynomials or other interpolative methods.

In photogrammetry this approach is denoted by "self-calibration", the concept is related to the method of so-called "collocation" (Moritz, 1973). An elementary implementation is by solving first a parametric formulation. This will be done in a least-squares method that leaves residuals at the observed image points. The residuals are then subject to an interpolative computation. This is meaningful only when the residuals form a systematic pattern. A new point $P(x_p, y_p)$ is thus converted to object coordinates by first adding Δx_p, Δy_p to x_p, y_p, and by then applying the radar equations.

2.5 Projection Of A Ground Control Point Into A Radar Image

In the event that the exterior orientation is measured, e.g. with the help of inertial navigation, one must expect errors of measurement to exist. These require correction with the help of ground control points.

Figure 2.9 illustrates the solution to the computation of the image coordinates x, y for a given object point $P(p_x, p_y, p_z)$ as it was published by Leberl, Fuchs and Ford (1981). The exterior orientation is known in the form of position vectors $\underline{s}_i$, $i=1,\ldots,m$ at times t_i, $i=1,\ldots,m$. Also given is thus the velocity vector $\dot{\underline{s}}_i = \underline{s}_{i+1} - \underline{s}_i$, or the equivalent attitude vector describing $\phi(t)$, $\kappa(t)$.

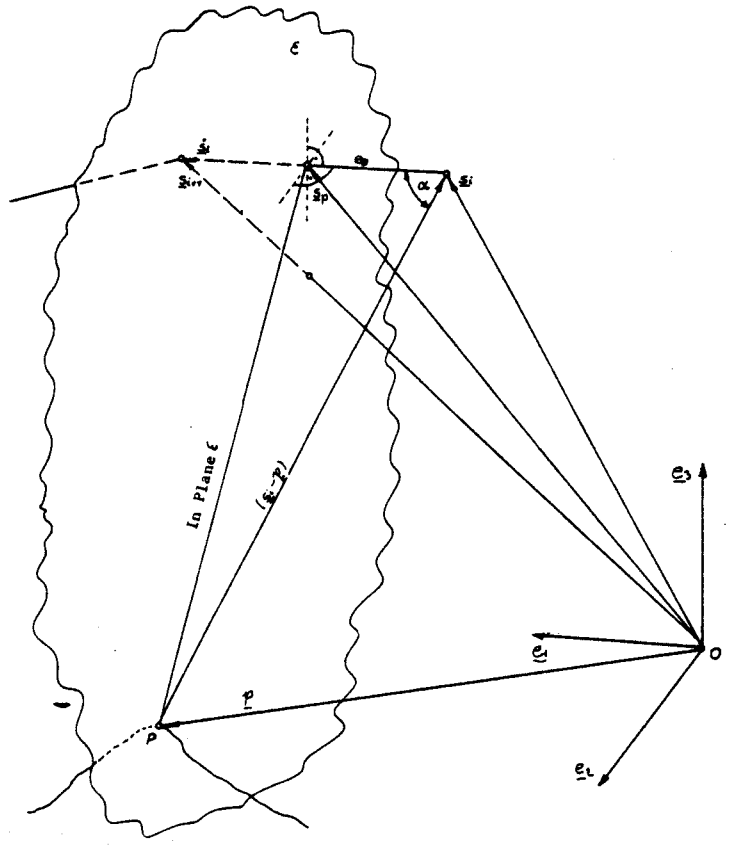

FIGURE 2.9: Computation of flight positions $\underline{s}_p$ at which ground point P was imaged.

From Figure 2.9 one finds:

$$(\underline{s}_i - \underline{p})\cdot\dot{\underline{s}}_i = |\underline{s}_i - \underline{p}|\cdot|\dot{\underline{s}}_i|\cos\alpha_i$$

where α_i is the angle between the linear orbit element i and the vector from $\underline{s}_i$ to $\underline{p}_i$. It relates to entity e_g:

$$\cos\alpha = e_g/|\underline{s}_i - \underline{p}|$$

where e_g results from:

$$(\underline{s}_i - \underline{p})\cdot\dot{\underline{s}}_i = |\dot{\underline{s}}_i|\cdot e_g, \quad e_g = \dot{\underline{s}}_i\cdot(s_i - \underline{p})/|\dot{\underline{s}}_i|$$

With this we get orbit position $\underline{s}_p$:

$$\underline{s}_p = \underline{s}_i + \dot{\underline{s}}_i\cdot e_g/|\dot{\underline{s}}_i| \qquad (2.25)$$

Position $\underline{s}_p$ then leads to slant range r_p and time t_p of imaging:

$$r_p = (\underline{p} - \underline{s}_p) \qquad (2.26)$$

$$t_p = t_i + |\underline{s}_p - \underline{s}_i|\cdot(t_{i+1} - t_i)/|\underline{s}_i| \qquad (2.27)$$

Actual image coordinates x_p, y_p are obtained through an inversion of the equations of inner orientation:

$$\bar{x}_p = x_i + (t_p - t_i)(x_{i+1} - x_i)/(t_{i+1} - t_i)$$

$$\bar{y}_p = r/f - c$$

Here, x_i, x_{i+1} are image x-coordinates of time references t_i, t_{i+1}.

These computed image coordinates can be compared with actual measurements of x, y. Discrepancies are the consequences of errors of inner and exterior orientation:

$$\Delta x = x - \bar{x}$$

$$\Delta y = y - \bar{y}$$

The Δx, Δy-discrepancies in control points can be used to compute correction functions and then to compensate for these errors in new points. The correction functions can be of the types as described in section 2.4.1.

2.6 Rectification

In orthophoto-generation by both digital image processing and photogrammetric computer assisted orthoprojection, one needs to define a sufficiently dense, geometrically correct grid of anchor points according to Figure 2.10. These anchor points are generated using rigorous radargrammetry. All image details inside a quadrangular grid mesh are transformed with a simpler and thus faster linear method.

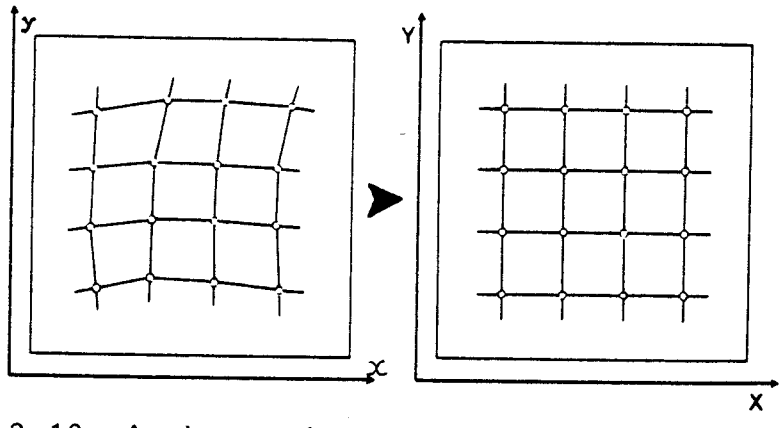

FIGURE 2.10: Anchor points in the deformed image (left) and orthophoto (right) (from Kraus, 1976).

The process is based on a raster DHM at orthophoto anchor points. These terrain points are resected onto the image according to Eqs. (2.25) to (2.27), so that a situation as shown in Figure 2.10 results. Based on these image coordinates one of the standard digital or analog photogrammetric rectification routines can be applied.

Rectified aircraft radar images were obtained from a study by Leberl and Fuchs (1978), and by Leberl, Fuchs and Ford (1981) with a detailed error analysis. Its discussion here would go beyond the scope of this report.

Digital rectification has been done so far in the context of the SEASAT-mission. Curlander et al. (1981) have used digital SAR-images from SEASAT together with orbital data, and Naraghi et al. (1981) matched the SAR-data with a digital terrain model.

Instead of actually creating a geometrically corrected radar image one can think of converting only certain interpreted image details to a map projection. If a DHM exists with the image and the image is related to the ground height through a computation of exterior orientation, then one can trace the image lines of interest with a digitizer; the image x, y-coordinates are transformed to X, Y knowing Z. This concept was realized by Greve and Cooney (1974) with radar, and is a method of photogrammetry which has also been proposed by other authors (e.g. Makarovic, 1973).

The idea has not yet had responses of any significance, either with metric photography or with radar or other image types. Interpretation of image contents apparently relies on the use of the stereo impression so that a pure single-image approach is not accepted even with existing DHMs.

2.7 Past Accuracy Studies

Numerous authors have compared single radar images to maps, thereby employing one of the described computing methods. An example of an early effort was by Leberl (1972a), as shown in Figure 2.11. Various interpolative methods were used to describe the image deformation.

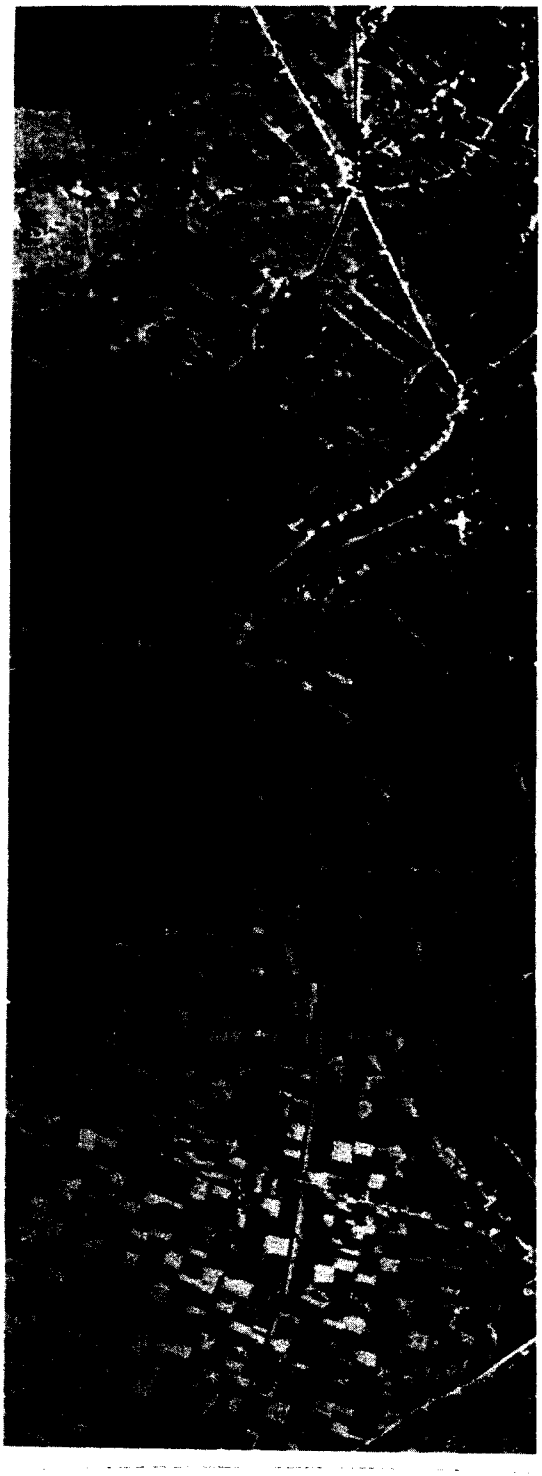

FIGURE 2.11: Example of a data set for an early single image accuracy elevation. British real aperture radar flight (1965) over Noord-Oost-Polder, the Netherlands, and map at scale 1:50 000 for comparison.

Table I is a review of some existing work. In view of the many possible mapping methods, of variations in the image types, of input data available on the terrain etc., it is obvious that a comparison of results is nearly impossible. However, one conclusion can be drawn, the range of achievable results stretches from the geometric ground resolution (Gracie et at. 1970) to some large figures. Clearly, though these larger figures may be caused by unknown topographic relief, lack of ground control points or poor internal geometry.

Expectations were expressed in the preparation phase of satellite radar that it could result in higher image geometry performance than aircraft radar (Leberl, 1976b). SEASAT-SAR was the first data to potentially prove that expectation. However, the overall system engineering for SEASAT-SAR did not optimize geometric performance. Table II presents results obtained with SEASAT-SAR. Hardcopy images on film either from optical or from digital correlation provided the same accuracy. Time and range referencing was not of sufficient quality to fully capitalize on a relatively stable orbit geometry and the resulting good geometric potential (Leberl et al. 1981). Without any ground control no meaningful positioning of ground points was feasible. With one or two such points the positioning error is ± 300 to 400 m.

TABLE I

Single image radargrammetric performance results (from Leberl, 1976b)

Source	Year	Accuracy (meters) along 1σ	Accuracy (meters) across 1σ	Relief	Control per 100 km²	Resolution (ground-meters)	Antenna Stabilized	Antenna Type	Radar system code	Scale of images 1:	Area designation, remarks
Gracie	1970	20	14	Flat	10.0	17	Yes	Synth.	AN-APQ 102		Atlanta, Georgia
Leberl	1971	50	23	Flat	10.0	30	No	Real	EMI (U.K.)	200 000	Netherlands
Bowman	1971	47	60	Flat	10.0	30	No	Real	EMI (U.K.)	250 000	Netherlands
Konecny	1972	152	255	Mount.		17	Yes	Real	Westinghouse	216 000	N. Guinea – conf transformation
Greve	1974	35				≥3	Yes	Synth.	TOPO II	100 000	Dig. monoplotting
Goodyear	1974	38	30	Flat	3.0	12	Yes	Synth.	GEMS 1000	400 000	Phoenix, Arizona
Derenyi	1974	89	111	Hills	1.1	17	Yes	Real	Westinghouse	250 000	Washington, D.C.
DBA-Systems	1974	51	26		0.5	3	Yes	Synth.	AN-ASQ 142	100 000	Radar interferometer
Konecny	1975	80	79	Flat		12	Yes	Synth.	GEMS 1000	400 000	Phoenix – conf transformation
Derenyi	1975	30	28	Flat		12	Yes	Synth.	GEMS 1000	400 000	Phoenix – control density not spec
Tiernan	1976	209	257	Flat	0.7	30–150	No	Synth.	Apollo 17	1 Mill.	Lunar satellite
Leberl	1976	147	233	Flat	0.3	30–150	No	Synth.	Apollo 17	1 Mill.	Lunar satellite
Hirsch	1976	120		Flat	3.0	30	No	Real	EMI (U.K.)	100 000	Netherlands
Leberl	1976	140	190	Flat	0.3	25–150	No	Synth.	JPL L-band	500 000	Alaskan tundra – sat. radar simul.

TABLE II

SEASAT-SAR geometric accuracy. Coordinate errors in km after radargrammetric measurements and computation, using the arctic passes over Banks and Victoria Islands taken by SEASAT covering 35 000 km², and pass 351 over Los Angeles

No. of control points	Rigorous radar-grammetry		Simple scale fit	
	x	*y*	*x*	*y*
Sea arctic images of Banks Island, 35 000 sq km				
1	0.45	0.49	—	—
2 (at both ends)	0.33	0.26	0.37	0.37
17	0.17	0.16	—	—
Image over Los Angeles, 7 pts per 100 sq km				
Optical corr.	0.024	0.017	—	—
Digital corr.	0.022	0.012	—	—

The rigorous use of digital imagery enables one to more fully exploit the data geometrically (Brown et al. 1981). Each pixel can be associated with a precise sensor events time and a slant range between antenna and object. As a result the location of an object on the Earth's surface can be computed without any ground control point to within several hundreds of meters. For the case of SEASAT, there is thus little difference between the use of rigorous radargrammetry and coarse approximations, except for the total lack of ground control or the presence of merely one or two points. For more appropriate mapping applicability a satellite radar would have to be equipped with precise time and range references and would need to be accompanied by accurate satellite orbit data with errors smaller than the geometric resolution of the sensor.

3.0 DESCRIPTION OF A SYSTEM FOR DIGITAL RADAR IMAGE RECTIFICATION

3.1 General

Input to a system for radar image rectification consists of:

- a digital radar image,
- sensor interior orientation parameters,
- sensor position and attitude values,
- ground control points,
- a raster digital elevation model (DEM).

In the current context one has to use the input to first create a mathematical relationship between image and map and then to actually create a rectified image. Many alternatives could be defined. The system developed under this study is based on the assumption that

- images exist of mountainous areas,
- identification of ground control points is difficult.

Therefore the system is based on radar image simulation to support the generation of a precise correspondence between radar image and object coordinates.

Radar image simulation with DEMs is only meaningful in the case of mountainous terrain; in flat areas a simulation as used here would be redundant.

A simulation system SIMRISA (Simulation of Radar Images using an Image Space Algorithm) has been developed and used for radar stereo analyses (Domik, Leberl and Raggam, 1983). It is extended to serve for rectification in the current effort.

3.2 Radar Rectification Based On Simulation

The procedure used for the rectification of radar images of mountainous terrain consist of the following steps:

(a) Generation of a digital elevation model, either from a map or from other external sources, or from radar stereo mapping;

(b) Verification and improvement, or computation of, sensor position and attitude parameters based on identifiable ground control points;

(c) Using the outputs of steps (a) and (b), i.e. a DEM, radar imaging parameters and a flight path, create a simulated radar image to resemble the given input image;

(d) Correlate the real and the simulated radar image, either by pointing to homologue features or by automated correlation, thereby creating a grid of anchor points in the real radar image to relate to the simulated one and consequently to the object coordinate system;

(e) Using a warping function, correct the real image to fit over the simulated image;

(f) Generate a geometrically rectified real image by assigning the real image gray value associated with the simulated pixel to each DEM grid cell;

(g) By substraction of the real image gray values from the simulated image one obtains a radiometrically corrected output image.

The above steps imply that an extensive software and radar image processing system is available. In fact the system needs to consist of various separate elements. In the current context one has:

- DEM generation by the Graz Terrain Model (GTM) system which takes given map contour lines to create a raster DEM;

- System for stereo mapping with radar techniques (SMART) to extract contour lines or raster

DEM data from stereo radar imagery on a photogrammetric analytical plotting machine (Kern DSR-1);

- Radar space resection programs to compute the flight parameters from a given input image and ground control points;

- Image processing programs for image correlation display and coordinate extraction;

- General purpose rectification based on a grid of anchor points (RECTIF);

- Radar image simulation (SIMRISA);

- Assignment of gray values to DEM grid cells based on an address file as a result of correlating the real with the simulated image (GEOREC).

The large set of required software for this purpose was envolved over the years in a sequence of individual efforts. The following will describe some of the more relevant components, in particular the method of DEM generation from stereo radar images and the radar image simulation.

For an overview of data and programs see Table III.

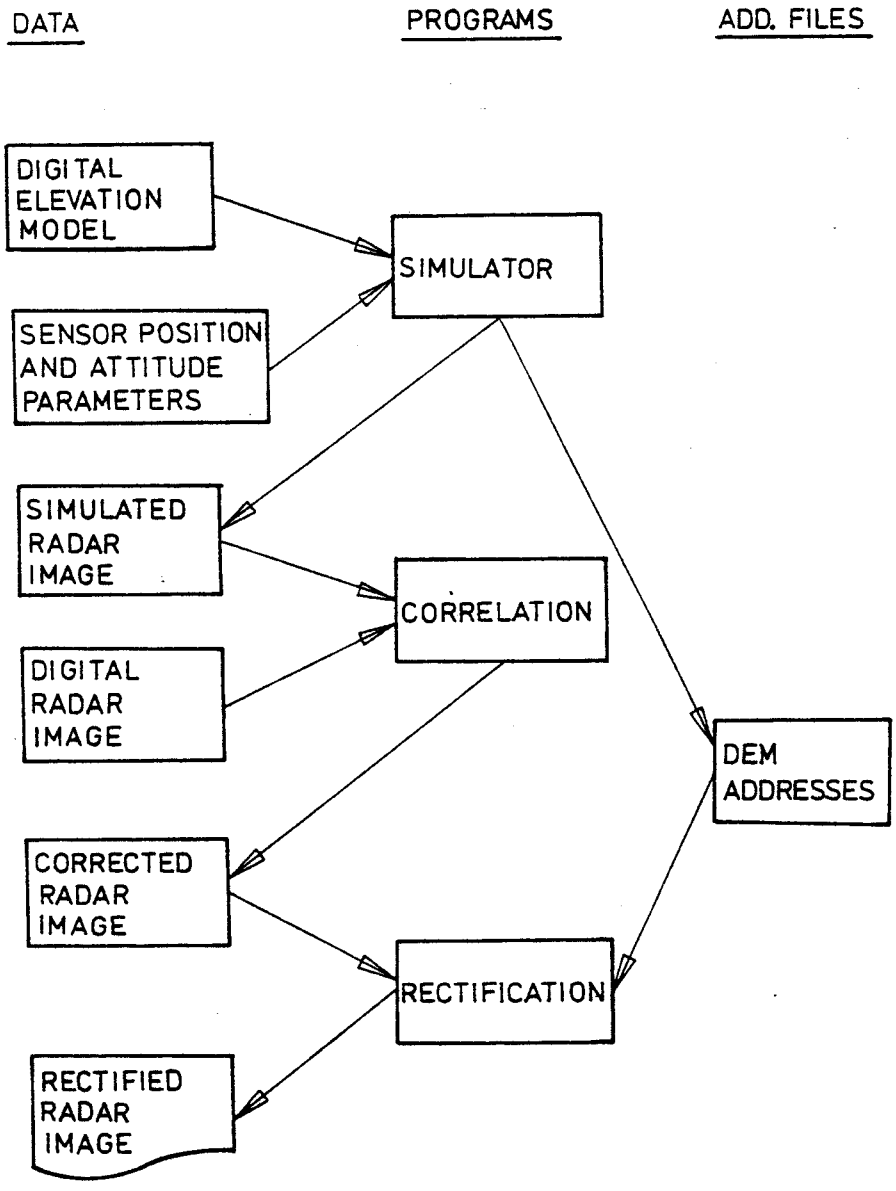

TABLE III: Diagram of program and data flow for a multi step approach of digital radar image rectification.

4.0 GENERATING A DEM WITH RADAR STEREO MAPPING

4.1 Background

Modern photogrammetric analytical plotters have opened up the possibility to employ other types of images than metric aerial photography for stereo-plotting. Instead of a fixed mechanical or optical analogon for the projection ray one has a flexible computer to relate image xy-coordinates to the cartesian XYZ object or model system.

Norvelle (1972) probably was the first to actually program an analytical plotter for stereo radar. The flexibility of earlier analytical plotters was hampered by the available computers and the use of low-level programming languages. Prior to Norvelle's work stereo-radargrammetry was developed in the context of basic studies, e.g. by Rosenfield (1968) and Gracie et al.(1970), and had led to a rather unique and specific radar stereo mapping instrument (Yoritomo, 1972; Graham, 1972).

The current generation of analytical plotters employs general purpose computers, distributed processing and high level programming languages. Therefore the effort required to program them is much reduced when compared to the early systems. This fact is combined with an increased interest in radar remote sensing as documented by satellite and other radar imaging experiments. Therefore it appears increasingly meaningful to study radar stereo mapping.

In an effort to demonstrate the flexibility of current commercial analytical photogrammetric instruments and in order to explore more fully the capabilities and limitations of stereo radargrammetry a procedure and software system for the analytical plotter Kern DSR-1 was developed to set-up, and plot from, radar stereo models. This is a first and preliminary report on this development, emphasizing a broad description of the procedures of SMART -- Stereo Mapping with Radar Techniques.[1)]

The chapter will discuss the procedure and demonstrate

---

1) This development was done outside the supported part of the current project DAJA45-83-C-0018. It is reviewed here due to its interest to the radar rectification and for ease of reference; see also Raggam and Leberl (1984).

it with a unique data set. Common radar image acquisition is with parallel flight lines. It is an added complexity to use intersection flight lines. As will be shown the DSR-1 is able to handle this type of data and produce a digital terrain elevation model of an accuracy commensurate with the radar input.

4.2 Overview Of System Modules

The programs for stereo radar are organized in separate modules. The entire process of model set-up follows radargrammetric formulations presented earlier and reviewed by Leberl (1983). Essentially the procedure requires sufficient ground control for the transformation of radar coordinates to the object space. The individual images are processed first to obtain approximate values for the rigorous radargrammetric solution. In the terminology of classical photogrammetry one first solves resections in space for the two images to then continue with a bundle adjustment using both images simultaneously.

Should no ground control be available then one has to work with given or assumed parameters of the flight path and sensor attitude. The preliminary resections would be skipped.

(a) Information and Initialization Module: This task enables the input and manipulation of initial project and image parameters. It serves for general information for the operator, such as for example project name, available images for the project or image and orbit data information.

(b) Control Point Management Module: This module is for the input and manipulation of ground control point data. The ground coordinates are in an orthogonal cartesian coordinate system, usually referenced to an origin within the area to be mapped and the Z-axis pointing along the local vertical of the origin.

(c) Orbit or Flight Data Management Module: This is for input and manipulation of sensor position measurements. The system assumes the orbit or flight to be represented with time polynomials so that sensor positions $\underline{s}$ may be expressed as follows:

$$\underline{s} = \underline{a} + \underline{b} \cdot t + \underline{c} \cdot t^2 + \ldots\ldots$$

where t is the time. Approximations for the orbit coefficient vectors ($\underline{a}$, $\underline{b}$, $\underline{c}$, ..) will be determined in the orbit data management module. Input are the position measurements, output is an array of polynomial coefficients. Joint low-order polynomials will be used instead of higher order polynomials if the need exists.

(d) Single Radar Image Processing: This module represents the equivalent of a resection in space to compute the orientation parameters for a single radar image with inner and exterior orientation. Plotting with a single radar image may be done on either a spherical surface of chosen radius or in a three-dimensional X, Y, Z - coordinate system with known constant Z.

(e) Stereo Radar Image Processing: This module includes the actual set-up of a radar stereo model. It follows the use of the single radar image module to determine approximations of the exterior orientation parameters of the two overlapping images. After elimination of y-parallaxes this module serves to plot contour-lines or planimetric features. Results are either directly plotted on an xy pen plotter or are entered into a digital data base for further processing. One example that is currently operational is for digital terrain elevation models with the Graz Terrain Model (GTM) program system (Oswald, Raetzsch, in print).

4.3 Radar Stereo Model Set-up

As previously described the radar stereo model set-up in SMART is realized in two steps consisting of the computation of the elements of inner orientation of the radar image pair, followed by an exterior orientation with a

radar bundle adjustment.

Inner Orientation: The inner orientation requires the establishment of a relationship between plate or image x, y coordinates and the physical radar measurements of time t and slant range r (see section 2.3). The system uses a so-called 'range reference line' at the near range edge of the image; it would correspond to the start of the sweep on the image recorder. It should be defined by some distinct tick marks (fiducials). In the event that no such marks exist the operator has to create artificial marks and determine the inner orientation in a process of self-calibration together with the exterior orientation.

Exterior Orientation: Measurement of homologue orientation points can first of all be as in a comparator by removing manually the x- and y-parallaxes. Secondly after a preliminary resection with each image one is in a nearly parallax-free stereo model and observation of homologue points is made more convenient. In contrast to analog stereo photogrammetry the analytical plotter does not need a relative orientation task seperate from absolute orientation. The parameters of relative and absolute orientation are found simultaneously with a so-called bundle adjustment. In our system this approach is the one used for radar images. The basic equations for the radar stereo adjustment consist of two types:

(a) The squint angle condition (see EQ. 2.10):

$$\underline{\dot{s}}\cdot(\underline{p}-\underline{s}) - \sin\tau\cdot|\dot{s}|\cdot|\underline{p}-\underline{s}| = 0 \qquad (4.1)$$

(b) The range condition (see EQ. 2.9):

$$r_s - |\underline{p}-\underline{s}| = 0 \qquad (4.2a)$$

for slant range presentations, or

$$\sqrt{r_g^2 + H^2} - |\underline{p} - \underline{s}| = 0 \qquad (4.2b)$$

for ground range presentations.

Each measured point gives rise to two equations of type (4.1) and (4.2). In addition each pair of homologue image points produces one additional condition. This is called the cocircularity condition, which defines the location of

an imaged point in object space by the intersection of two circles, each defined by two equations of type (4.1) and (4.2). The equations are non-linear. Linearized forms are used in an iterative solution.

Observations for the computations are sensor position measurements, image coordinate measurements of ground control points in one or in both images and pairs of homologue image coordinate measurements of stereo model orientation points. Unknowns to be determined within the adjustment are:

- the coefficients of the orbit time polynomials;
- the radar imaging parameters (inner orientation) to convert radar image coordinates to range and time;
- the parameters of a correction polynomial to describe radar image deformations;
- a value for the squint angle.

The solution for the unknowns in each iteration of the non-linear equation system is obtained in the instruments host processor in a least squares adjustment using the method of conjugated gradients (Schwarz, 1970). This solution method is iterative and may have some advantages for larger equation systems when a small computer must be used and both computing times and storage requirements are limited. Furthermore there is evidence that the method is more robust for this special problem than a strict Gauss solution of normal equations.

Depending on the quality of the approximate values the adjustment process must be repeated iteratively until results satisfy specified termination criteria.

4.4 Example Of Radar Stereo Plotting With SIR-A Satellite Data

A Space Shuttle Imaging Radar SIR-A stereo image pair of the Greek islands Cephalonia and Ithaka was used to illustrate the procedure of extracting a digital height model (Fig. 4.1). A more detailed study of the stereoscopic computations from such data is presented by Kobrick et al.(submitted). Viewing limitations were discussed by Domik et al.(1983). After model set-up the topographic elevations were digitized in the object coordinate system using profiles and ridge lines; the measurements were entered into the terrain model system GTM. The GTM program enables one to generate contour line plots at chosen interval, to obtain axonometric views of the terrain data and various other products.

Figure 4.2 shows an axonometric view of the digital elevation model (DEM) of the islands extracted from a map 1 : 200 000, Figure 4.3 presents the DEM created on the Kern DSR-1 analytical stereoplotter. A comparison of the two DEM's is possible with the GTM-system and reveals that the root mean square differences over all DEM points of the islands amount to $\pm$ 98 meters.

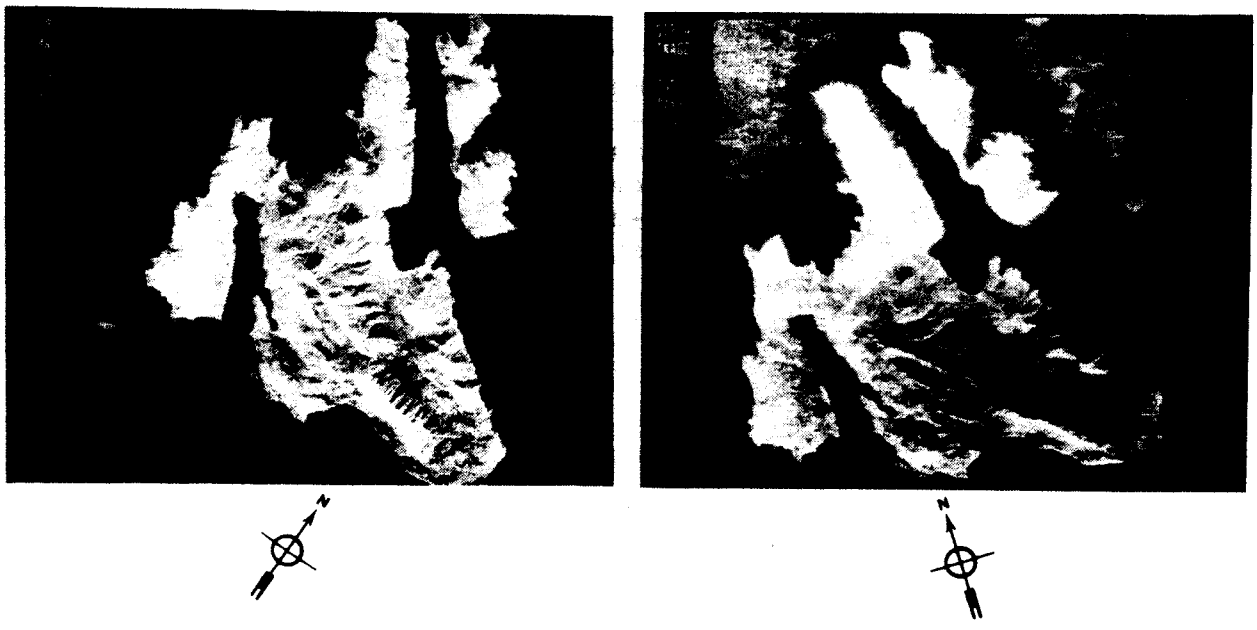

FIGURE 4.1: Space Shuttle Imaging Radar SIR-A stereo radar image pair of the Greek islands Cephalonia and Ithaka, taken at 34° angle between flight lines at 45° look angle off-nadir.

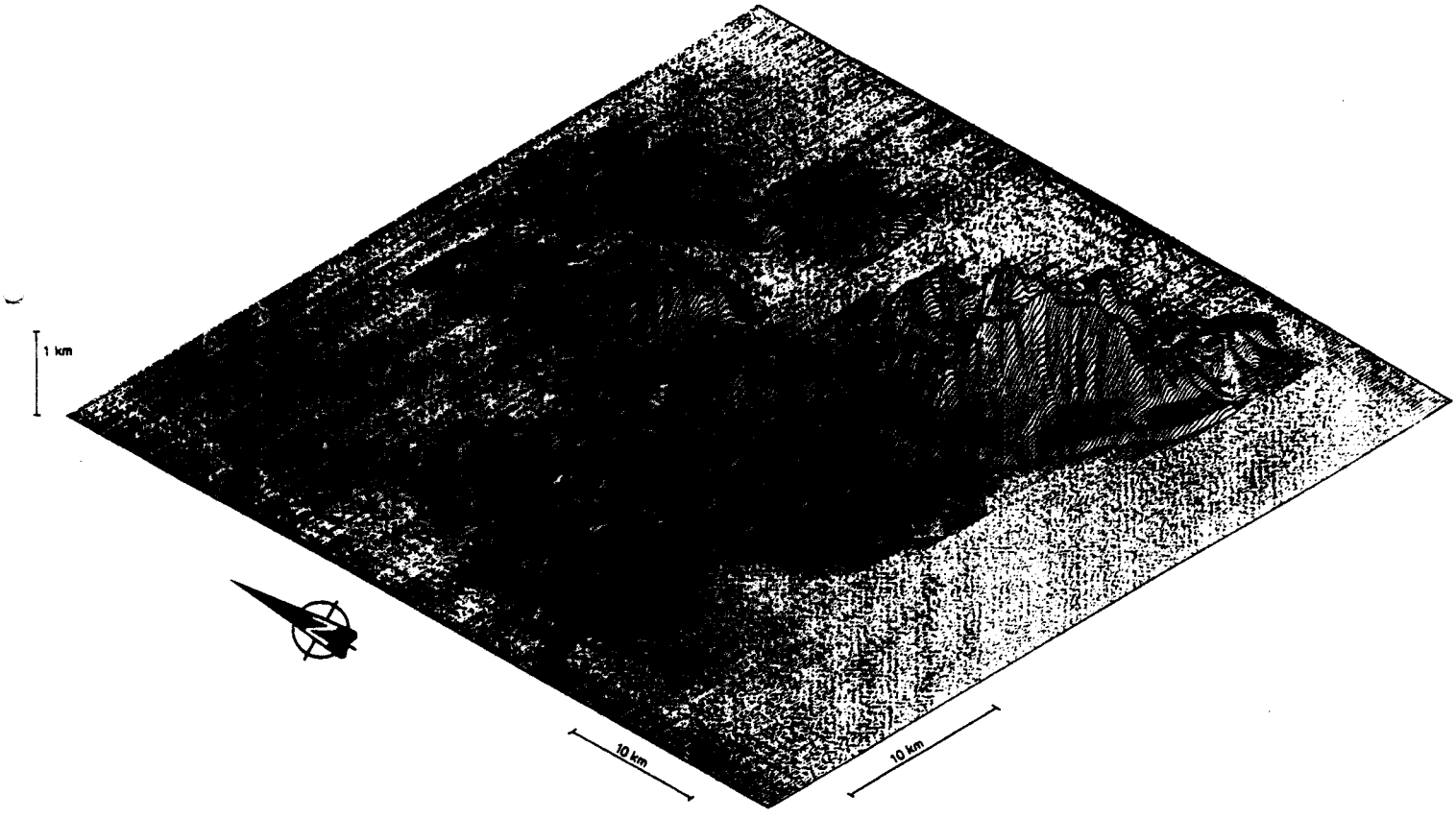


```
*********************************
   CEPHALONIA AND ITHAKA        *
  DATA FROM MAP 1 : 200000      *
*********************************
```

FIGURE 4.2: Digital elevation model of the Greek islands Cephalonia and Ithaka in axonometric view. Data are extracted from a map 1 : 200 000, raster interpolation is by system GTM.

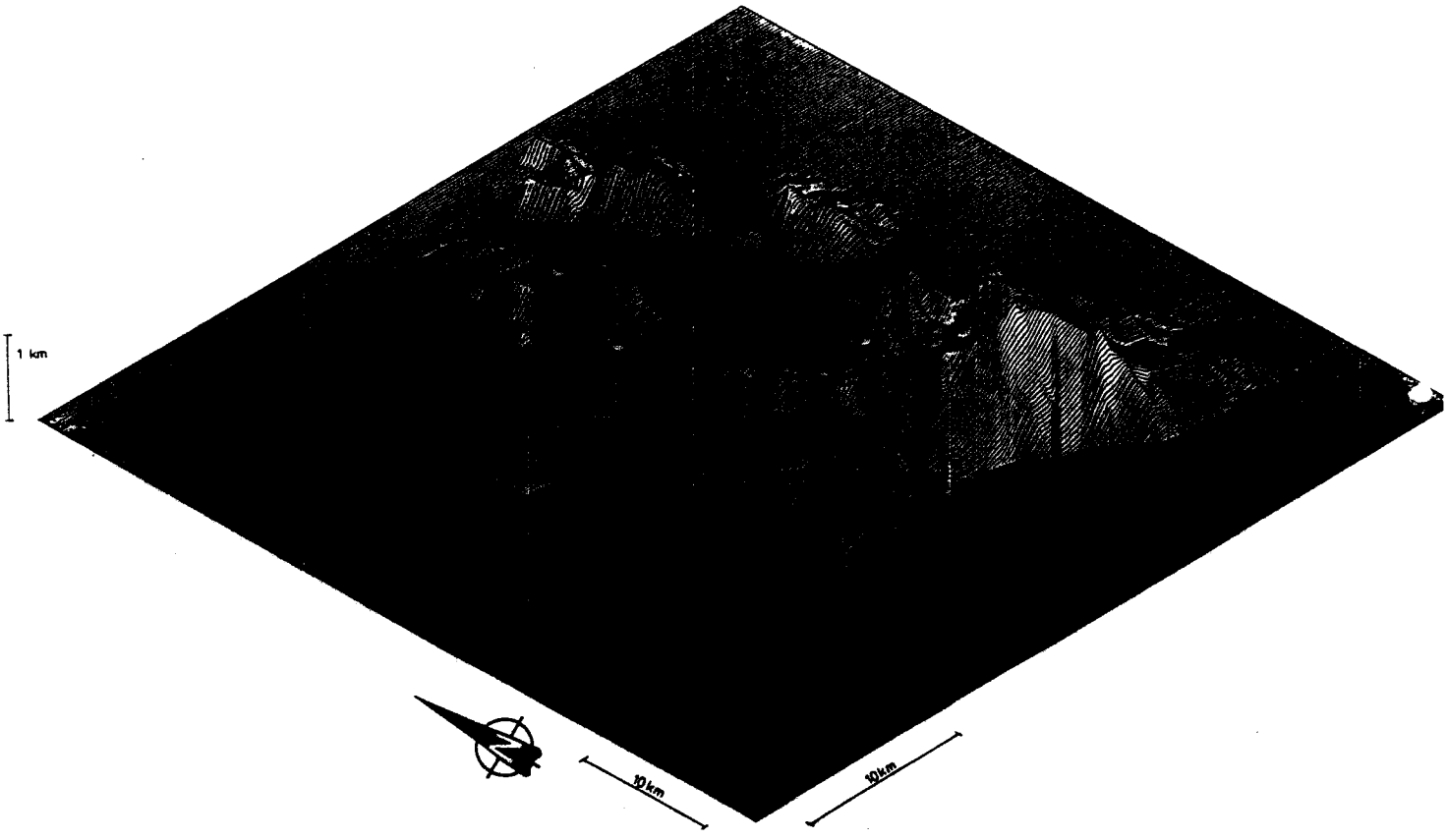


```
*************************************
*      CEPHALONIA AND ITHAKA        *
*   DATA GENERATED AT KERN DSR-1    *
*************************************
```

FIGURE 4.3: Digital elevation model of the greek islands Cephalonia and Ithaka in axonometric view. Data digitized at KERN DSR-1 stereoplotter using program SMART.

4.5 Software Implementation

The software package is currently installed at a Kern DSR-1 analytical plotter under the name SMART (Stereo Mapping with Radar Techniques).

The DSR-1 standard configuration consists of three independent digital processing units, which are denoted as P1, P2 and P3 (Chapuis, 1980). Processor P1 is the host computer. It serves for development and execution of application programs and performs data transfer between the other processors. The computation of set-up parameters for the radar stereo model is done in P1. Processor P2 receives the radar image orientation parameters from P1 and uses them to convert in real time model coordinates X,Y,Z to radar image coordinates r',t',r",t" and onto DSR-1 plate coordinates x',y' and x",y". P2 also transfers image, model or object coordinates to processor P1 if requested. Processor P3 is an added convenience for the operator and controls an operator control panel which may be used for communication between operator and DSR-1.

The Kern DSR-1 therefore uses three computers as opposed to other plotters which may employ only one. What seems to be an added complexity in fact is an advantage: the real-time operations are performed by a seperate processor P2 with a clearly defined software interface for a user working with the host P1. The user will therefore work in a familiar, general purpose multi-user environment with an unmodified operating system. The critical real time operations are singled out.

5.0 RADAR IMAGE SIMULATION

Approaches to image simulation can be categorised according to the domain of the transformation function. Object space algorithms map each object point (DEM point) into a two dimensional field (image) whereas image space algorithms start from equidistant image coordinates (i,j) of the output image and assign gray value accordingly to it. Object space algorithms are usually faster in their application than image space algorithms. But there is a need for interpolation to convert the unequally spaced image addresses to equidistant ones.

The development of the radar simulation was part of another project (see Domik, Leberl and Raggam, 1983). It is of great relevance in the current context and is discussed in the following for ease of reference.

An image space algorithm was chosen to be implemented because it provides DEM addresses at exact image locations. Fig. 5.1 and 5.2 show the basic idea of object vs. image space algorithms.

Gray values are attached to the image coordinates dependent on the corresponding incidence angle on the ground.

5.1 The Geometric Imaging Model

The image coordinates (i,j) serve as start values for the simulation program. They are used to extract imaging time t and slant range r or ground range g by Eq.'s 5.1.

$$t = (i-1)*f_i + t_0 \qquad \text{EQ.(5.1a)}$$

$$r = (j-1)*f_j + s_d \qquad \text{EQ.(5.1b)}$$

$$g = (j-1)*f_j + s_d$$

$$r = SQRT(H^2 + g^2) \qquad \text{EQ.(5.1c)}$$

where

t....imaging time of coordinate (i,j)
t_o...start time of imaging
f_i...scale factor in azimuth-direction
f_j...scale factor in range-direction

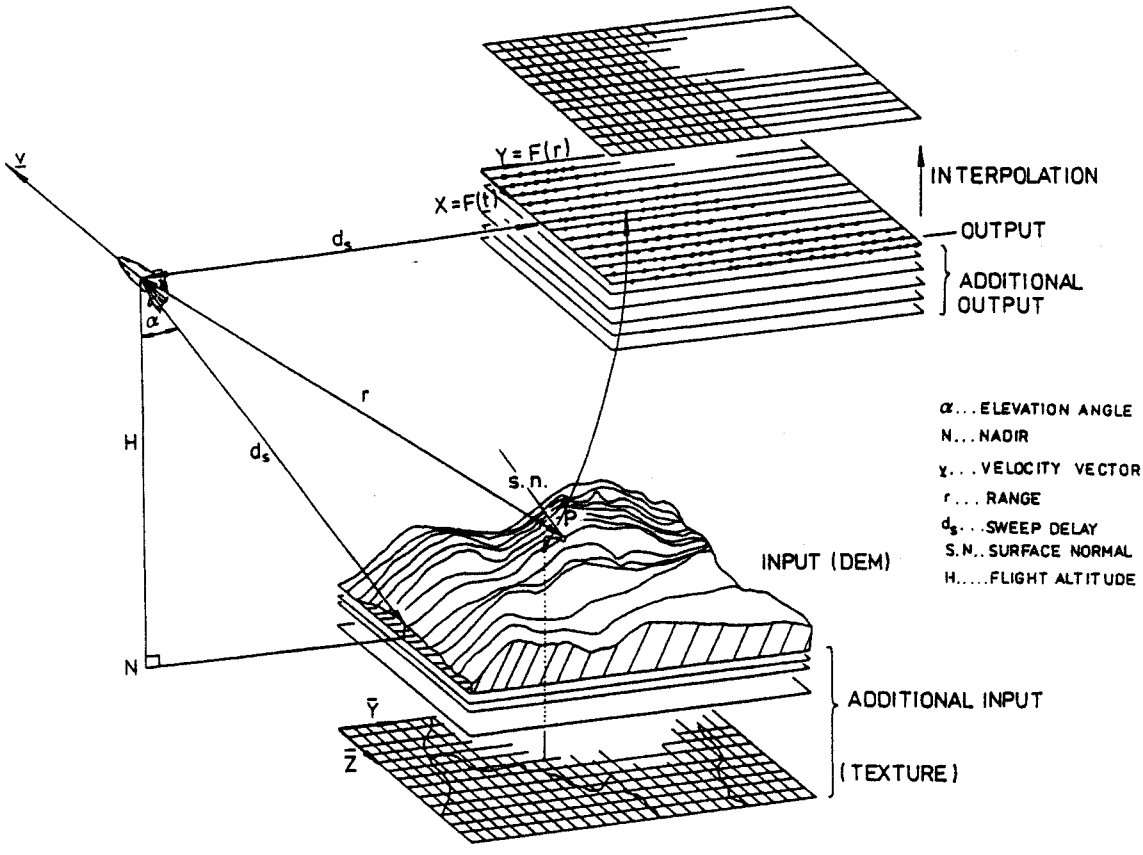

FIGURE 5.1: Object Space Algorithm: Projecting from the ground (object space; presented by a digital elevation model) into the image space.

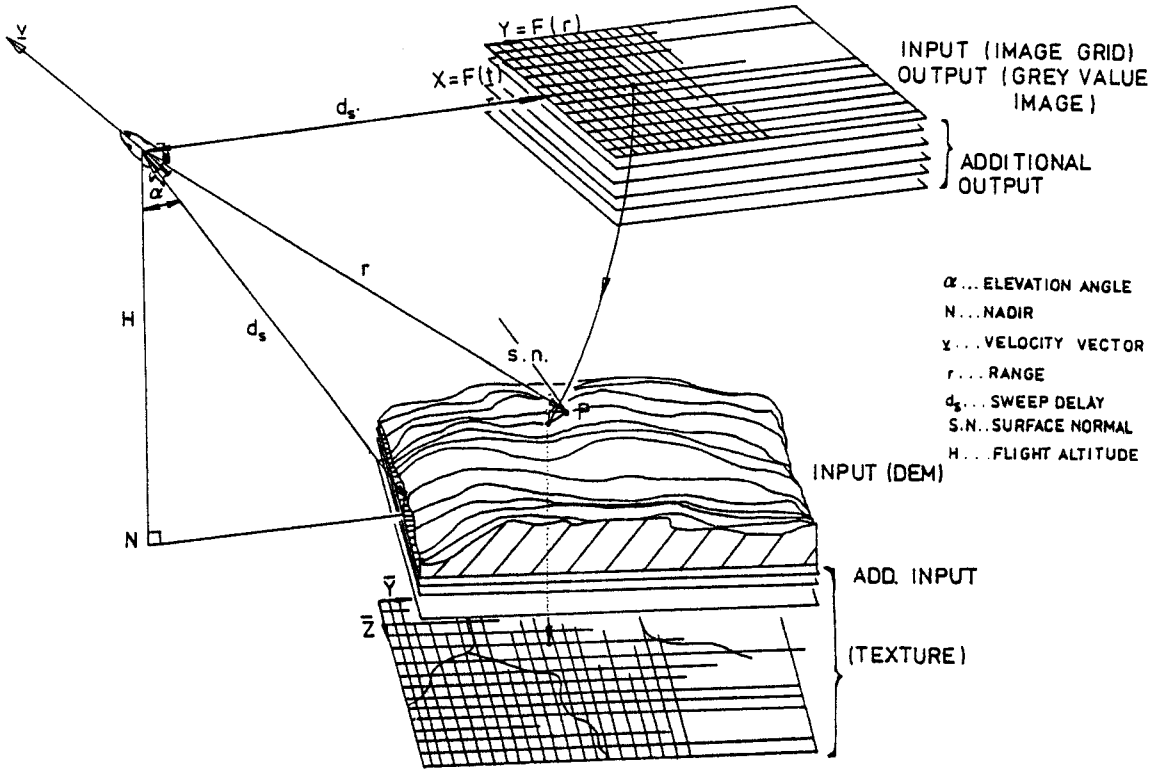

FIGURE 5.2: Image Space Algorithm: Projecting from equidistant image coordinates (image space) down to the ground.

The sensor position and velocity vector, derived from the imaging time, define a cartesian coordinate system: The sensor position is the origin of this "sensor coordinate system", the axes are defined by the velocity vector and the sensor position as expressed in a geocentric coordinate system (Eq. 2.8). The set-up of this system allows a clear presentation of the geometry created by any input coordinate (i,j).

The origin of the sensor coordinate system is the center of a sphere with radius r (range sphere). In general, a squint angle $\tau \neq 0$ is assumed for imaging. Thus a cone is defined with the peak in the origin and its axis along the velocity vector of the air- or spacecraft. All generating lines form an angle of $(90^{o} - \tau)$ with the axis. If the squint angle τ is equal to 0 imaging is in a plane perpendicular to the velocity vector. The intersection of sphere and cone, or, sphere and plane, respectively, defines a circle (intersection circle). The remaining task is now to intersect the circle with the DEM.

At least one intersection point but possibly several ones will be found. The occurrence of more than one solution is called "lay-over": different terrain targets were illuminated simultaineously. The address of each intersection point as well as corresponding look angle, surface inclinations and additional informations are stored for further processing.

5.2 Radiometric Model Of Imaging

The definition of an image gray value in a given pixel location is denoted as "radiometric model". One has to define areas of shadow (black), confuse reflection, multiple reflection in lay-overs etc.

Black image areas are mostly shadows or water bodies. In order to find those pixels that indeed are shadow areas one has to sort the look angles

going from near range to far range along an imaged object line. Shadow areas begin where an increasing range r is associated with a reduced look-angle off nadir.

In areas other than shadows the image gray value is a function of the incidence angle for the incoming radiation. This is an angle between the line of sight antenna-object and the local normal onto the surface.

Once this angle is computed for a pixel one has the choice of selecting a back scatter curve according to the thematic charactaristics of the material and of the reflection angle τ. Standard backscatter function are those of Hagfors (1964), Muhleman (1964) or a cosine-function.

Simultaneous illumination of various terrain parts leads to image lay-overs: the projection circle intersects more than one point on the ground. The gray value is the sum of the individual reflection values.

5.3 Data Structure

The internal data structures are constructed to make available a fast access to the address file elements in relation to the image elements. Each azimuth line in the image represents a logical block and corresponds to a unique logical block of the address file. Memory allocation for each logical block will be a minimum of n*e bytes, where n is the number of range columns and e the number of bytes used for storage of one gray value. The address file allocates (at minimum again) h*f bytes, with h being the number of addresses belonging to one azimuth line and f the number of bytes used for one address definition. The relation is realized by an additional access-matrix (pointer file), which allows a fast association between elements of the two different files. The additional storage for the relation matrix will be h*2 bytes per logical block.

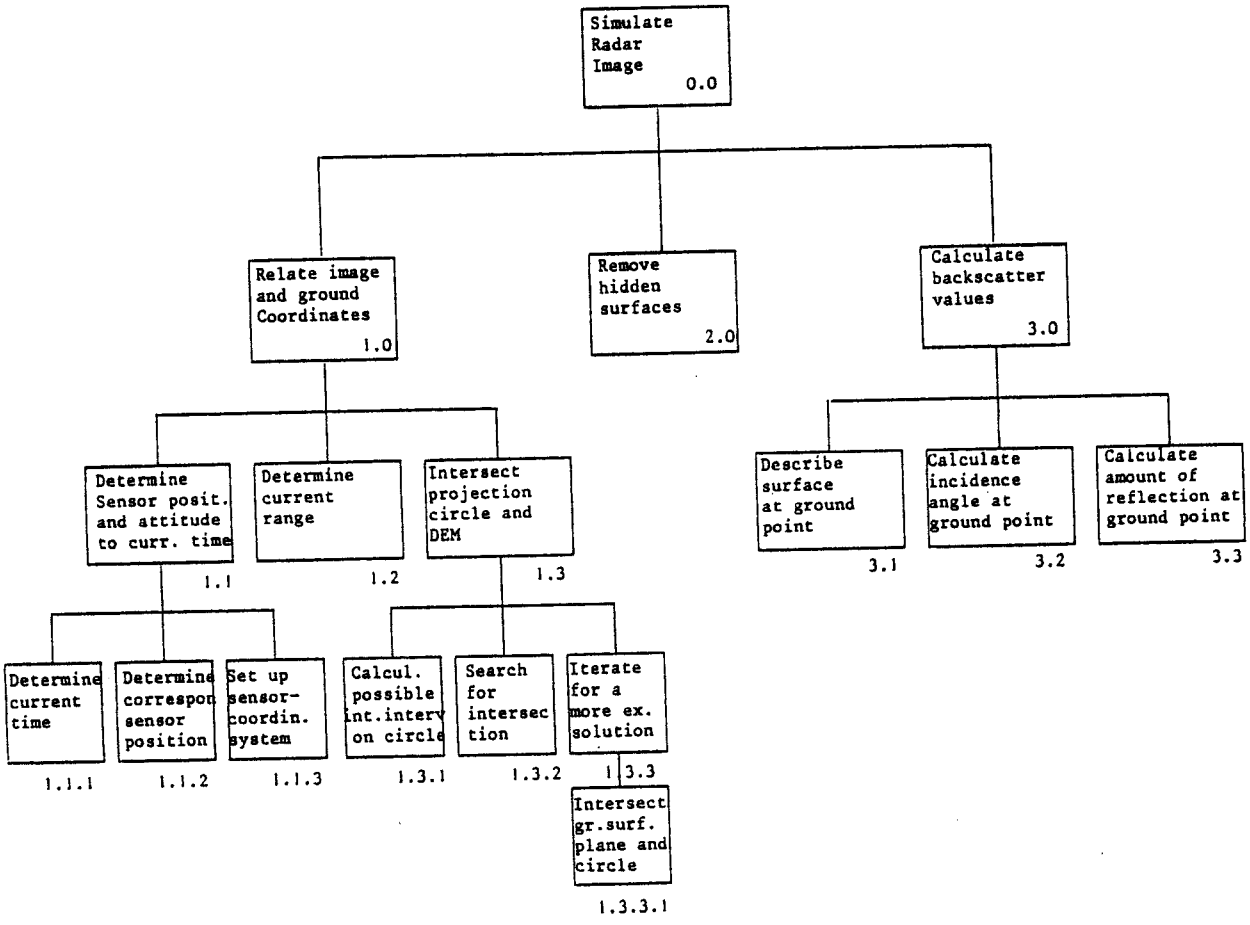

FIGURE 5.3: Table of contents for the software package SIMRISA. End leaves present more detailed description.

5.4 Software Implementation

The product of the software implementation to perform the simulation is named SIMRISA (SIMulation of Radar images using an Image Space Algorithm) and is currently running on a VAX-11/750.

Emphasis was put on modularity of the system (see description of system modules, Fig. 5.3). The program can be easily changed, e.g. additional thematic input data sets could allow for use of different backscatter curves or use of different look-up tables within one DEM area.

6.0 OTHER AUXILIARY SYSTEM ELEMENTS

6.1 Registration

The image registration is based on a program RECTIF by Diarra (1982); it is a modular software system for geometric correction of an image. Input is a set of homologue pairs of points whose coordinates are known in the real image and in the simulation. These are used to compute correction polynomials to describe the trend of the image deformations. Residuals at control points serve then to compute refined corrections with some higher order interpolative method. Work is thus via "warping" or "rubber-sheeting". Polynomials are limited to degree 3 or less, so that they are both stable and overdetermined. Residuals are extracted at each anchor point, and serve to modify the original polynomials.

These correction polynomials are used for resampling based on a grid of anchor points; each set of object coordinates obtains image-positions. Various methods may then be applied to determine gray values at those positions: interpolation followed by nearest neighbor assignment, bilinear interpolation, and bicubic interpolation, are the current options. Control points will usually be defined by hand, or by digital correction.

The registration results in a rectified image; in the case of data actually studied remaining distortions are of an average of 3 pixels or less, assuming an appropriate distribution of control points.

This results in a real radar image superimposed onto the simulated data.

6.2 Removing Geometric Radar Distortions

Any gray value occuring in the digital radar image is characterized by:

- the gray value number (brightness) of the pixel;
- the location of the pixel in the image.

The gray value is a function of incidence angle, wavelength, polarisation and reflecting capability of the corresponding targets. With fixed wavelength and polarisation the brightness varies only with incidence angle and reflection properties.

The location of the pixel in the image is defined by the time delay of the radar pulse to and from the target. For a perfectly flat ground the time delay increases proportional to the distance of nadir and target. Irregularities on the surface to be imaged affect the time delay and create distortions in the image.

An extreme effect of relief displacement occurs with lay-over; the top of a target to be imaged is closer to the radar sensor than the bottom and is therefore recorded sooner. However, lay-over is also defined as the simultaneous mapping of two different ground targets into one resolution cell. This is the case when the slant range of two objects is the same. Lay-over effects the brightness as the return power from two or more targets is added up. The simulation process can correctly consider the lay-over case by attaching more than one position address to an image gray value.

After the simulation and registration each digital DN number of the corrected radar image is connected to one or more DEM addresses. The procedure GEOREC (GEOmetric RECtification) performs the final step of the radar image rectification making use of the data structures described in chapter 5.3.

Input to this last step are

- grey values of the real image registered to the simulation

- address file (containing DEM addresses)

- relation between grey values and address file

According to the data structure description the logical blocks of grey value and address file correspond sequentially to each other. This allows to process each azimuth line (corresponding to one logical block) independently. Each gray value is now placed at the DEM addresses calculated during the simulation. Thus the geometric radar distortions are eliminated again and the resulting ortho image displays distances instead of (slant or ground) ranges.

Usually the DEM-addresses are not exact grid positions, so that some kind of interpolation has to take place.

7.0 EXAMPLES OF RADAR IMAGE RECTIFICATION

7.1 Oetztal-Data

A radar image was obtained during the European SAR-580 campaign of the Oetztal in Tyrol (Rott, 1983). The sensor for this mission was carried aboard a Convair-580 aircraft with a dual band, dual polarisation SAR which could be operated in X and C band or X and L band. Data were recorded by using either an optical or a digital recorder:

The aim of the Tyrol-part of the SAR-580 experiment were investigations in the applications of radar for mapping snow and glaciers in mountainous regions. The sensor was operated in X and C band (HH polarisation), covering a ground swath of 13 km length. Fig. 7.1 is a presentation of the SAR image, X band, recorded digitally and processed at the German Aerospace Research Establishment (DFVLR). The presentation is in ground range; the original resolution of 3 m was changed to a coarser resolution of 24 m for presentation in 512 x 512 pixels.

A DEM was derived from a map 1 : 50 000 by scanning the contour and drain/ridge lines. The imaged part is only a subarea of the DEM, which extends from $10^{\circ}48'$ to $10^{\circ}59'$ East longitude and from $46^{\circ}45'$ to $46^{\circ}52'$ North latitude. The mountain spreading from the south-western towards the north-eastern corner can be recognized in the radar image (upper half). The illuminated digital height model of the area to be investigated is presented in Fig. 7.2.

FIGURE 7.1: Airborne radar image (SAR-580): X-band, HH polarisation, flight altitude 6 km; ground range presentation. Oetztal, Tyrol, Austria.

FIGURE 7.2: Illuminated height model. The radar image presents a subset of this area.

7.2 Processing Of The Oetztal Data

The simulation was carried out by the simulator according to chapter 5. Since flight navigation was eroneous during the SAR-580 flight, one has to rely on control points to approximately derive the flight and imaging parameters. The maximal height in this area is 3615 m, whereas the minimal height is 85 m. Hagfors law was used to model the backscatter depending on the incidence angle. No additional input was used to distinguish between different thematic features in the image.

The simulation results in a gray value image with an additional address file and relation matrix. The gray values assigned by the simulator are merely functions of the incidence angle and do not consider any properties of the imaged targets (Fig. 7.3).

The geometry created by the simulation matches the real image closely. The radar distortions due to radar properities like forshortening and shadowing are correctly implemented by the simulation.

However, sensor dependent errors will be present due to the inaccurate flight and imaging records. Thus there is a need for geometric image correction. The registration described in chapter 6 creates a modified radar image to fit with the simulated one. The simulated image serves to support control point definition.

The corrections applied to the real radar image are shown in Fig. 7.4. Corresponding features in both real and simulated image were used as control points in the registration. Their residual vectors are plotted into the deformation grid with a 10 x 10 pixel size. The DN values of the new SAR image (Fig. 7.5) may now replace the synthetic gray values and correspond to the additional output files of the simulation. Thus the connection between radar image and DEM addresses is made and the rectification can be carried out by the appropriate procedure.

The radar ortho image is shown in Fig. 7.6.

FIGURE 7.3: Simulated radar image: approximated flight path and elevation model serve as input. Ground range presentation and diffuse scattering are assumed.

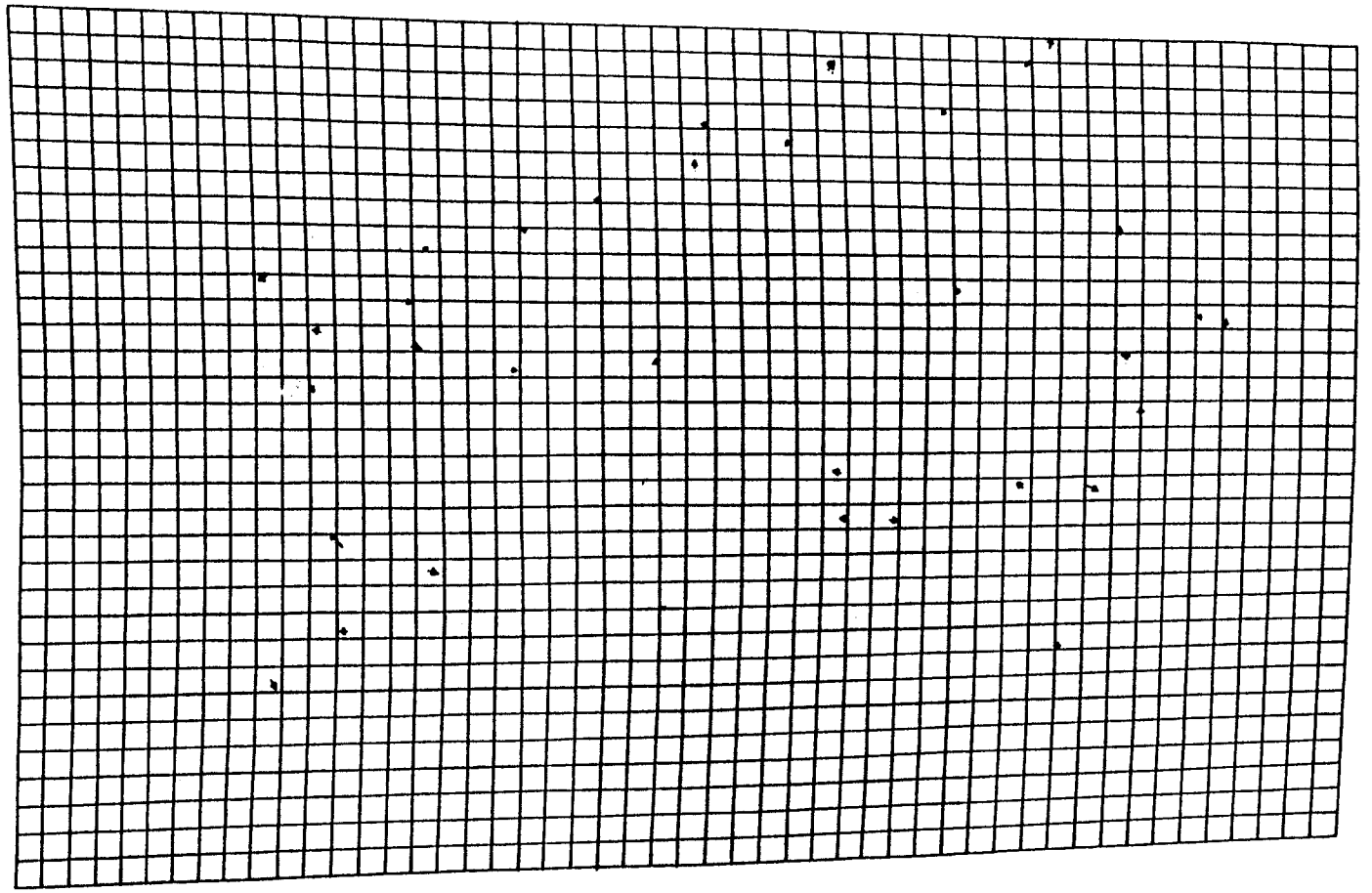

FIGURE 7.4: Grid showing geometric distortions between real and simulated image. Anchor points and residual vectors are plotted in the grid. One grid cell lenght corresponds to 10 pixels.

FIGURE 7.5: SAR-580 image corrected in its geometry to the simulation using the distortion grid.

FIGURE 7.6: Radar ortho image: Image containing the backscatter information from the radar image but with the geometry of a map (undistorted image).

The simulation displays the gray values as a function of the incidence angle, whereas the gray values in the real image vary with the change of incidence angle <u>and</u> thematic characteristics. Substracting the simulated gray values from the real data leaves a radiometric corrected image (Fig. 7.7): Those parts in the image, which are mainly influenced by the surface inclination are displayed in middle gray tones, parts where the thematic content enhances the return power are to be distinguished by a lighter gray to white. Dark gray tones indicate the strong reflection in the simulation as compared to the real image. Especially near the edges of the image the dark tones are largely insignificant.

FIGURE 7.7: Radiometrically corrected radar image: Influence of topography in radar brightness is removed.

7.3 Cephalonia Data

On Nov. 12, 1981, the SIR-A (Shuttle Imaging Radar-A) was launched aboard NASA's space shuttle. SIR-A is a left-side-looking SAR operated at L-band frequency with an elevation angle of approximately 50° off nadir to the center of the imaging swath. SIR-A data were optically recorded.

Two images obtained in Europe from Data Take 32-33 and Data Take 37A, resp., were of special interest for stereo investigations (see Fig. 4.1). Though SIR-A was not specially designed for stereo-investigations, several data takes from crossing orbits proved to deliver fairly well stereo. The intersection angle of the imaged swaths was approximately 34°.

For our investigations the images presented on film were scanned by an Optronics device to receive the data in digital form. The digital data was processed to receive a resolution of approximately 100m.

The analog images were used to create a stereo-derived elevation model as explained in chapter 4. At the same time an elevation model was genereated by digitizing the contour-lines at a 200 m interval of a 1 : 200,000 map in UTM projection. Axonometric presentations of both models are presented in Fig. 4.1.

7.4 Processing Of Cephalonia Data

The process is analog to the Oetztal data processing, using the modules of the radar image processing system described in chapters 4 to 6.

Flight and imaging information to be entered into the simulation were gained from (Cimino and Elachi, 1982): Latitude and longitude for the center of the swath as well as flight altitude were recorded only for each minute, so the flight path was approximated by a straight line at the height of about 264 km (slightly descending). The STC position and the interpulse period were used to calculate the sweep delay to the near edge of the swath. The image presentation was in slant range. Through the simulator a synthetic radar image was created from the stereo-derived DEM together with an additional address file (Fig. 7.8). The registration resulted in Fig 7.9 by removing the differences (see registration grid in Fig. 7.10) between real and simulated image. The final ortho image (Fig. 7.11) was created by resampling the radar image grey values at their corresponding DEM addresses.

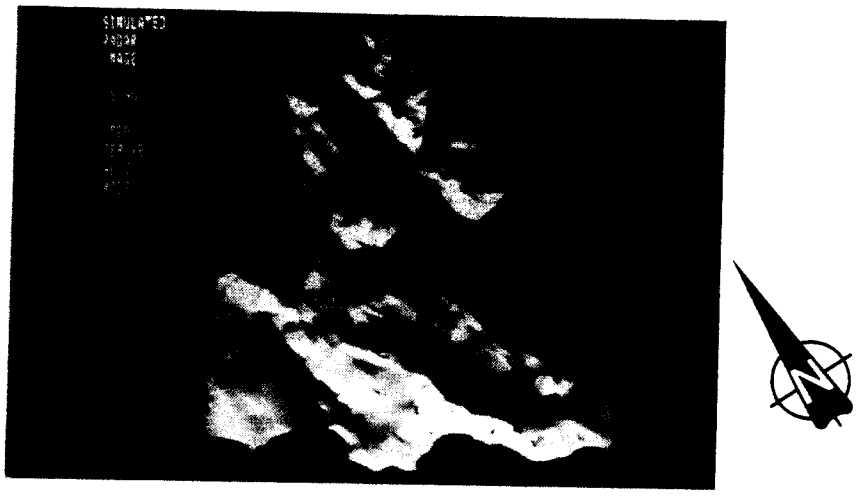

FIGURE 7.8: Simulated radar image using imaging and sensor parameters from the SIR-A recordings and stereo-derived elevation model.

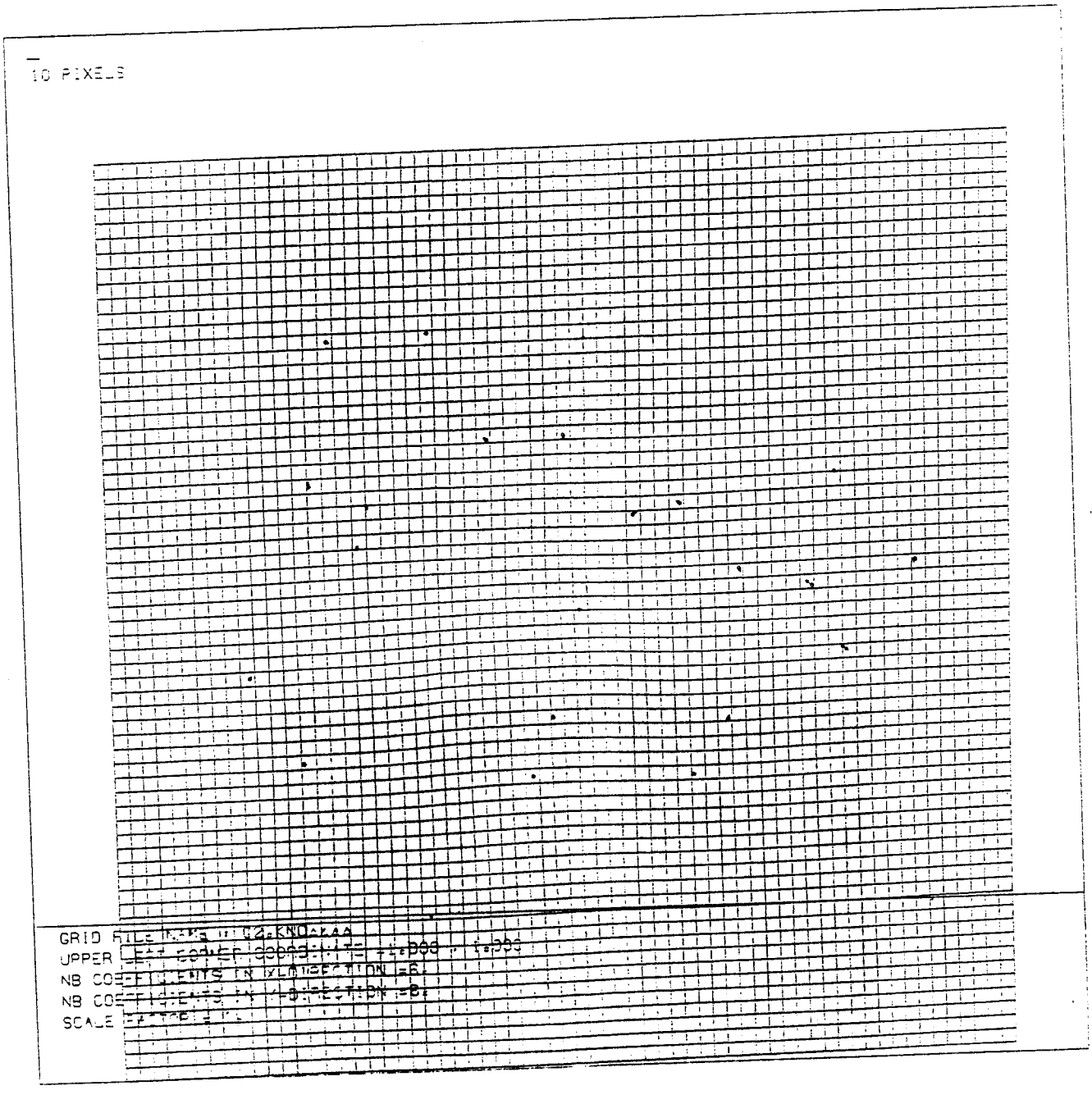

FIGURE 7.10: Distortion grid between real and simulated image. One grid cell lenght corresponds to 10 pixels. Anchor points and residual vectors are plotted in the grid.

FIGURE 7.9: Geometric differences between simulated and real image are removed in this radar image.

FIGURE 7.11: Radar ortho-image created from a SIR-A image (Date Take 37A) using the height model derived from the radar stereo pair of two SIR-A images with a crossing swath (Data Take 37A and 32-33).

8.0 CONCLUSION AND OUTLOOK

We have described an elaborate software system for the rectification of digital radar images. Rectification is based on digital elevation models from maps or from radar stereo models, on control points and on given data of the sensor and flight path.

The core of the procedure is an image simulation to support the identification of homologous features in both the image and the DEM. Rectification can be geometric and/or radiometric.

The entire system is experimental: the size of manageable data sets is limited, required computing resources are significant. In order to improve the current system one has to speed up the processes and to gain more experiences with both the simulation and the rectification. Simulations must improve to consider thematic variations, and to more distinctly be sensitive to geometric resolution.

A question of great concern is the matching of images from different sources, such as Landsat-MSS, -TM and radar. It is thus clear that great efforts will still be required to expand current capabilities so that they include the concepts of multi-map correspondence and multi-resolution analysis.

AKOWETZKY W.I. (1968): "On the Transformation of Radar Coordinates into the Geodetic System". Geodezia i Aerofotojomka (in Russian).

BROWN W. et al. (1981): "Application of Seasat SAR Digitally Correlated Imagery for Sea Ice Dynamics". Invited Paper, 1981 AGU-Meeting, Baltimore, USA.

CHAPUIS A. (1980): "Das Kern System DSR-1/GP-1. Analytisches Stereo-Auswertegeraet und graphisches Peripheriegeraet". 14th ISP Congress, Commission II, Hamburg 1980.

CURLANDER J. (1981): "Geometric and Radiometric Distortion in Spaceborne SAR Imagery". Invited Paper, NASA Workshop of Registration - Rectification for Terrestrial Applications. November 17 - 19. Jet Propulsion Laboratory, Pasadena, USA.

CURLANDER J. (1981): "Sensor to Target Range Determination". IPL-Interoffice Memorandum 334. 7-80-056. Jet Propulsion Laboratory, Pasadena, USA.

DBA SYSTEMS (1974): "Research Studies and Investigastions for Radar Control Extensions". DBA Systems, Inc., P.O. Drawer 550, Melbourne, Florida, Defense Documentation Center Report No. 530784L.

DERENYI E.E. (1970): "An Exploratory Investigation into the Relative Orientation of Continuous Strip Imagery". Ph.D. Thesis and Research Report No. 8, Univ. of New Brunswick, Canada.

DERENYI E.E. (1974): "SLAR Geometric Test". Photogramm. Eng., Vol. XL.

DERENYI E.E. (1974): "Metric Evaluation of Radar and Infrared Imageries". Second Canadian Symp. on Remote Sensing, Univ. of Guelph, Guelph, Ontario.

DOMIK G., Leberl F., Raggam J.(1983): "Evaluation of Radar Stereoscopic Viewing". Final report on contract Nr. F49620-82-C-0053, European office of Aerospace and Development, London. DIBAG - Report Nr. 11, Graz Research Center, A-8010 Graz, 127 p.

DOWIDEIT G. (1977): "Eine Blockausgleichung für Abbildungen des seitwärtschauenden Radar (SLAR)". Wissensch. Arbeiten der Lehrstühle für Geodäsie etc., Nr. 75, Technische Universität Hannover, FRG, 185 pp.

DOWIDEIT G. (1977): "Eine Blockausgleichung für Aufzeichnungen des Seitwärts-Radar (SLAR)". Bildmessung und Luftbildwesen Vol. 45, No. 1, pp 17 - 23.

EBNER, H., and R. HOESSLER (1978): "The Use of Gauss-Markov Processes in Digital Rectification of Remote Sensing Data, ISP-Comm. III Sympos., Moscow, pp. 258-265

GEIER F. (1972): "Fundamentals of Orientation for Radar PPI Images with approcimated Horizontal Distances". Pres. Paper, 12th Congress, Int. Soc. Photogramm., Ottawa, Canada.

GRACIE G. et al. (1970): "Stereo Radar Analysis". U.S. Engineer Topographic Laboratory, Ft. Belvoir, Virginia. Report No. FTR-1339-1.

GREVE C. and W. COONEY (1974): "The Digital Rectification of Side Looking Radar". Proc. Am. Soc. Photogramm., Annual Convention, Wash., C.D.

GRAHAM L.C. (1972): "An Improved Orthographic Radar Restitutor". Presented Paper, 12th Congress, Int. Soc. Photogramm., Ottawa, Canada, and Goodyear Aerospace Corp., Report GERA-1831.

GUERTIN F.E., SHAW E. (1981): Definition and Potential of Geocoded Satellite Imagery Products. Presented Paper, 7th Canadian Symposium on Remote Sensing, Winnipeg, Manitoba, Sept. 1981.

HIRSCH TH. and J. VAN KUILENBURG (1976): "Preliminary Tests of the EMI-SLAR Mapping Quality". Netherlands Interdepartmental Working Community for the Appli. and Res. of Remote Sensing (NIWARS), Internal Report No. 39, Delft.

HOCKEBORN H.A. (1971): "Extraction of Positional Information from Side Looking Radar". Bildmessung und Luftbildwesen, Vol. 39, No. 1.

KRAUS, K. (1976): "Anwendungsmöglichkeiten eines digital gesteuerten Differntialumbildegerätes", Geowissenschaftliche Mitteilungen, No.8, pp.1-22, Technical University Vienna, Austria.

KOBRICK M., Leberl F., Raggam J.(submitted): "Convergent Stereo with the Shuttle Imaging Radar". Manuscript, Jet Propulsion Laboratory, MS 183-701, Pasadena, California 91109.

KONECNY G. and E.E. DERENYI (1966): "Geometric Consideration for mapping from Scan Imagery". Proc. 4th Symp. Remote Sensing of the Environment. Ann Arbor, Michigan.

KRATKY V. (1979): "SEASAT Orbit Effects on Imaging Geometry of Synthetic Aperture Radar". 3rd GDTA Symposium, Toulouse.

LEBERL F. (1970): "Metric Properties of Imagery Produced by Side Looking Airborne Radar and Infrared Line Scan Systems". Publications of the International Institute for Aerial Survey and Earth Sciences (ITC), Series A, No. 50, Delft.

LEBERL F. (1971): "Vorschläge zur instrumentellen Entzerrung von Abbildungen mit Seitwärts Radar (SLAR) und Infrarotabtastsystemen". Bildmessung und Luftbildwesen, Vol. 39.

LEBERL F. (1971): "Remote Sensing - Neue Methoden zur Wahrnehmung auf Abstand". Oesterreichische Zeitschrift für Vermessungswesen, No. 6.

LEBERL F. (1971): "Untersuchungen über die Geometrie und Einzelbildauswertung von Radarschrägaufnahmen". Diss., Techn. Univ., Wien.

LEBERL F. (1972): "On Model Formation with Remote Sensing Imagery". Oesterr. Zeitschrift für Vermessungswesen, Vol. 60, pp. 93 - 61.

LEBERL F. (1972): "Evaluation of Single Strips of Side Looking Radar Imagery". Arch. Int. Soc. Photogrammetry, Invited Paper, 12th Congress, Ottawa, Canada.

LEBERL F. (1972): "On Model Formation with Remote Sensing Imagery". Oesterr. Zeitschrift für Vermessungswesen und Photogrammetrie, No. 2.

LEBERL F. (1975): "The Geometry of, and Plotting from, Single Strips of Side Looking Airborne Radar Imagery". Int. Institute for Aerial Survey and Earth Sciences (ITC) Techn. Report No. 1, Enschede.

LEBERL F. (1975): "Radargrammetry for Image Interpreters". ITC Technical Report No. 2, Enschede.

LEBERL F. (1975): "Radargrammetric Point Determination PRORADAN". Bildmessung und Luftbildwesen, Vol. 45, No. 1.

LEBERL F. (1975): "Sequential and Simultaneous SLAR Block Adjustment". Photogrammetria, Vol. 31, No. 1.

LEBERL F. (1975): "Lunar Radargrammetry with ALSE-VHF Imagery". Proc. Am. Soc. Photogramm., Fall Tech. Meeting, Phoenix, Arizona.

LEBERL F. (1976): "Mapping of Lunar Surface from Side Looking Orbital Radar Images". The Moon, Vol. 15, No. 3/4.

LEBERL F. (1976): "Imaging Radar Applications to Mapping and Charting". Photogrammetria, Vol. 32.

LEBERL F., H. FUCHS (1978): "Photogrammetric Differential Rectification of Radar Images". Pres. Paper Symp. of Comm. III of the Intl. Soc. Photogrammetry, Moscow and Mittl. d. geod. Inst. No. 33, TU-Graz, 8010 Graz, Austria.

LEBERL F., H. FUCHS, J. FORD (1981): "A Radar Image Time Series". International Journal of Remote Sensing, Vol. 2, No. 2.

LEBERL F., J. RAGGAM (1982): "Satellite Radargrammetry", Phase I. Final Report. DIBAG-Report Nr. 4, Research Center Graz, Austria

LEBERL F., J. RAGGAM, M. KOBRICK (1983, in print): "Stereo Viewing of Radar Images". IEEE Trans. Geoscience Remote Sensing.

LEBERL F.(1983): "Photogrammetric Aspects of Remote Sensing with Imaging Radar". Remote Sensing Reviews, Harwood Academic Publishers, London. pp. 71 - 158.

MAKAROVIC B. (1973): "Digital Mono-Plotters". ITC-Journal 1973-4, ITC, Enschede, The Netherlands, pp. 583-600.

MORITZ, H. (1973): "Least Squares Collocation", Deutsche Geodätische Kommission, Series A, Nr. 75, München, W. Germany.

NARAGHI M., W. STROMBERG, M. DAILY (1981): "Geometric Rectification of Radar Imagery Using Digital Elevation Models". Image Processing Laboratory of the Jet Propulsion Laboratory, Pasadena, USA.

NORVELLE R.R. (1972): "As-11-A Radar Program". Photogramm. Eng., Vol. XXXVIII.

RINNER K. (1948): "Die Geometrie des Funkbildes". Austrian Academy of Sciences, Math. Naturwiss. Klasse, also in "Handbuch der Vermessungskunde", Jordan-Eggert-Kneissl, Vol. VI, Metzlersche Verlagsbuchhandlung, Stuttgart.

RINNER K., R. Burkhardt (1972): "Photogrammetrie", Band III a/1, Handbuch der Vermessungskunde, J. B. Metzler`sche Verlagsbuchhandlung, Stuttgart.

ROSENFIELD G.H. (1968): "Stereo Radar Techniques". Photogramm. Eng., Vol. XXXIV.

SCHWARZ H.R. (1970): "Die Methode der konjugierten Gradienten in der Ausgleichsrechnung". Zeitschrift fuer Vermessungswesen, Vol. 4/1970, pp. 130 - 140.

SHAKINE A., T. LE TOAN (1978): "A Study of Digitized Radar Images". Intl. Symp. of Remote Sensing of Environment, Ann Arbor, USA.

YORITOMO K. (1972): "Methods and Instruments for the Restitution of Radar Pictures". Arch. Int. Soc. Photogramm., Inv. Paper, 12th Congress, Ottawa, Canada.